ELSEVIER

Precambrian Research 71 (1995) 183–205

Precambrian Research

# Metamorphic events in the eastern Arunta Inlier, Part 1. Metamorphic petrology

Jo Arnold, Michael Sandiford, Simon Wetherley[1]

*Department of Geology and Geophysics, University of Adelaide, Adelaide, SA 5005, Australia*

Received 11 December 1992; revised version accepted 18 January 1994

**Abstract**

In the Entia Dome of the eastern Arunta Inlier kyanite-facies metamorphism is recorded over a substantial area (at least 160 km$^2$) and thus contrasts with the regionally extensive belts of high-temperature–low-pressure andalusite–sillimanite facies metamorphism documented elsewhere in the Arunta Inlier. This amphibolite facies event appears to postdate regional granulite facies metamorphism, evidence for which is almost totally obliterated. In the Entia Dome prograde kyanite occurs in meta-basites in comparatively rare associations involving hornblende, staurolite and anorthite, and in other rocks in association with gedrite and hornblende or garnet and biotite. These kyanite-bearing assemblages equilibrated at intermediate temperatures (570–710°C) at peak pressures of ~7 kbar and are overprinted by lower-pressure assemblages including hornblende–gedrite, cordierite and sillimanite. While this sequence of reactions may be simply interpreted in terms of a single "clockwise" orogenic cycle, textural evidence and the available mineral isotopic data suggest a more complex history involving multiple heating and cooling episodes during the Mesoproterozoic, and, possibly, the Palaeozoic. The occurrence of regional retrogressive kyanite-facies assemblages in the eastern Arunta Inlier provides evidence that the widely held perception that Proterozoic crustal evolution in Australia involved a distinct ensialic orogenic style characterised by high geothermal gradients (Etheridge et al., 1987; Loosveld and Etheridge, 1990; Sandiford and Powell, 1991) is not universally true. Rather, petrological evidence, presented here with isotopic constraints described by Foden et al. (1995), suggests that the Harts Range region has experienced substantial crustal reworking at elevated temperatures, during both the Proterozoic and Palaeozoic, under thermal regimes more familiar to modern continental collision zones.

## 1. Introduction

Any understanding of the pressure–temperature–time ($P$–$T$–$t$) evolution of a metamorphic terrane must rely heavily upon the interpretation of mineral assemblages, textures and mineral chemistry that preserve different stages of the metamorphic history. The occurrence of mineral associations indicative of particular thermal regimes has commonly been used to infer the common crustal processes involved in their formation. In this context a number of workers have suggested that a consistent style of metamorphism in the Proterozoic terranes of northern and central Australia involved high-temperature–low-pressure (andalusite–sillimanite facies) metamorphism and "anticlockwise" $P$–$T$–$t$ paths implying a common, widespread tectonic setting. High-temperature–low-pressure metamorphism

[1] Present address: Department of Geology, University of Western Australia, Nedlands, WA 6009, Australia.


*SSDI* 0301-9268(94)00061-1

has been implied for the Granites Tanami Block (peak conditions of 600°C, 3.5 kbar, Scrimgeour and Sandiford, 1993), the Broken Hill Inlier (peak conditions of 700–800°C, 5–6 kbar, Hobbs et al., 1984) and the Arunta Inlier (e.g. peak metamorphic conditions of $\geqslant$750°C, 2.5 and 5.5 kbar in the Anmatjira Range, Clarke et al., 1990; 680–780°C at ~4 kbar in the Reynolds Range, Dirks et al., 1991). Many of these terranes appear to have experienced several stages of this style of metamorphism, and they are often dissected by discrete kyanite-bearing retrograde shear zones (Warren, 1983; Clarke et al., 1990).

The mechanisms proposed for crustal evolution in the Australian Proterozoic accounting for this apparently ubiquitous high-temperature–low-pressure metamorphism involve ensialic orogeny. This is in contrast to the intercratonic setting which has been dominant during the Phanerozoic where higher $P/T$ metamorphism, indicative of lower geothermal gradients is more typical, though not exclusively so (Etheridge et al., 1987).

In contrast to the andalusite–sillimanite facies metamorphism, which is dominant in these Proterozoic Blocks, there is significant evidence that metamorphism in the eastern Arunta Inlier and in particular the Entia Dome, involved regionally extensive kyanite facies metamorphism at some time after the granulite facies event(s) preserved in other parts of the Inlier (Dobos, 1978; Warren, 1983; Goscombe, 1992b). The Eastern Arunta Inlier has therefore experienced a metamorphic history at least partly distinct from many other Australian Proterozoic terranes. Similarly Foden et al. (1988) have proposed that the felsic igneous rocks present in the Entia Dome differ markedly in their chemical signatures from the typically anorogenic magmas of the remainder of the Arunta Inlier and other Proterozoic terranes. Whereas typical Proterozoic granites are silicious with high Y, Zr, Nb, LIL and LREE contents, the Entia Dome granites are generally more Ca- and Sr-rich, with low Zr and Nb contents (i.e. they are more like modern volcanogenic or syn-collisional granites (Foden et al., 1988)).

The implications of prograde metamorphism under the influence of a significantly lower geothermal gradient in the eastern portion of the Arunta Inlier have been neglected by those who have attempted to generalise about Australian Proterozoic crustal evolution, partly because, until recently, the metamorphic history of the area had not been well documented. However, this very contrast with the northern Arunta Inlier and other Proterozoic inliers engenders considerable significance for the Entia Dome in future interpretations of the northern Australian Proterozoic terranes. In this paper we describe the metamorphic geology of the Entia Dome, concentrating on the northeastern region where a supracrustal assemblage contains a wide variety of mineral assemblages, including an unusual association of hornblende–kyanite–staurolite developed during amphibolite facies metamorphism.

## 2. Geology of the Entia Dome, Harts Range

The Arunta Inlier is one of a number of Proterozoic crustal blocks exposed in northern and central Australia, and outcrops over approximately 200,000 km$^2$ in the Alice Springs region (Fig. 1). It has been extensively mapped to the 1:100,000 scale by the BMR (e.g. Shaw et al., 1990), who proposed the stratigraphic divisions and structural provinces which have formed the basis of the knowledge of the Inlier (Stewart et al., 1984; Shaw et al., 1984). The Entia Dome is situated at the eastern end of the Arunta Inlier, approximately 180 km ENE of Alice Springs, in the Harts Range. The core of the 25 km wide dome comprises mainly felsic orthogneisses (Entia gneiss complex), interlayered with amphibolite bands which are of basaltic and intrusive origin (Foden et al., 1988). This is structurally overlain by a mylonitised granitic gneiss (the Bruna gneiss) and a supracrustal sequence (the Irindina supracrustal assemblage, Ding and James, 1985).

The Entia gneiss complex consists of a supracrustal assemblage including interlayered amphibolites, calc-silicates, carbonates, pelitic and

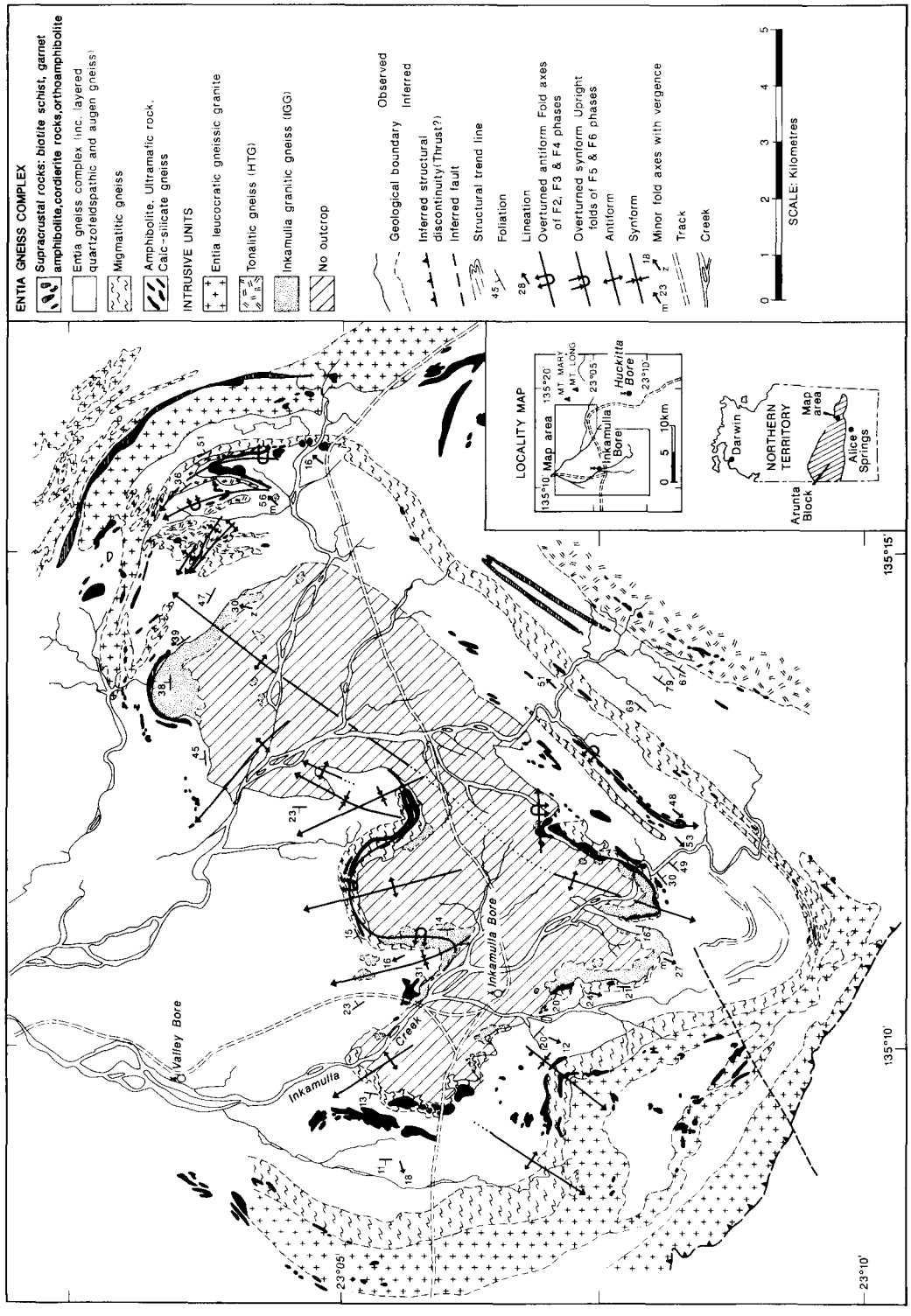


Fig. 1. Geological map of the northeast portion of the Entia Dome, after Foden et al. (1988). Samples were collected from the "supracrustal rocks" in the northeast of the area.

other metasedimentary rocks which were fragmented and dismembered by the intrusion of large granitoid sheets at $\sim 1767 \pm 2$ Ma (Cooper et al., 1988). These granitoids consist of three main bodies, the Huckitta granodiorite gneiss, the Huckitta tonalite gneiss and the Inkamulla granite gneiss (Buick 1983, 1985; Foden et al., 1988), which have been intruded by a younger set of amphibolite dykes and associated small layered intrusions (Foden et al., 1988).

The main fabric evident in the Entia gneiss complex is reflected in the pervasive amphibolite facies foliation and mineral lineation (Ding and James, 1985; James and Ding, 1988). The retrogressive nature of this fabric is evident in the occasional preservation of granulite facies assemblages in the cores of the boudins which are present at a range of scales (see Foden et al., 1995). Ding and James (1985) show that this dominant amphibolite fabric developed synchronously with compositional layering and is folded by a number of later fold generations, which, however, have not caused new foliations to develop. It is the petrology of these amphibolite facies assemblages which is the focus of this contribution, while Foden et al. (1995) discuss their isotopic characteristics. We note that Ding and James (1985) proposed that the Entia gneiss

Table 1
Whole-rock analyses

| Sample # | Ky-Bt-schist 853-76 | u.m. cum 950-081 | u.m. cum 950-089 | Crd-Oam 853-30 | amphibolite 962-017r | amphibolite 853-180 | amphibolite 962-155 | St-Ky-Ep-Hbl HR91-4 | Grt-St-Ep-Hbl HR91-8 | Grt-Hb-Bt 853-16 |
|---|---|---|---|---|---|---|---|---|---|---|
| % | | | | | | | | | | |
| SiO2 | 42.93 | 48.77 | 48.73 | 47.18 | 47.78 | 49.28 | 46.42 | 38.14 | 37.92 | 67.04 |
| TiO2 | 0.31 | 0.12 | 0.34 | 0.65 | 0.57 | 0.61 | 1.06 | 1.47 | 2.37 | 1.01 |
| Al2O3 | 34.84 | 5.71 | 7.62 | 26.53 | 23.99 | 14.62 | 16.29 | 19.41 | 20.78 | 11.05 |
| Fe2O3* | 5.23 | 7.86 | 14.13 | 7.57 | 6.83 | 9.59 | 13.59 | 16.45 | 17.25 | 9.03 |
| MnO | 0.05 | 0.16 | 0.21 | 0.12 | 0.10 | 0.16 | 0.20 | 0.24 | 0.16 | 0.12 |
| MgO | 11.8 | 27.41 | 22.19 | 15.9 | 5.33 | 9.91 | 7.67 | 8.29 | 6.37 | 3.26 |
| CaO | 0.55 | 4.19 | 3.96 | 0.43 | 9.11 | 14.02 | 11.90 | 11.60 | 11.04 | 6.17 |
| Na2O | 1.05 | 0.37 | 0.83 | 0.91 | 3.47 | 1.75 | 2.20 | 1.86 | 1.36 | 1.09 |
| K2O | 2.68 | 0.03 | 0.06 | 0.73 | 1.12 | 0.32 | 0.48 | 0.76 | 0.50 | 0.27 |
| P2O5 | 0.2 | 0.01 | 0.05 | 0.07 | 0.42 | 0.04 | 0.16 | 0.43 | 0.04 | 0.38 |
| LOI | 3.09 | 5.01 | 2.53 | 2.93 | 1.59 | 0.71 | 0.64 | 1.60 | 0.91 | 0.35 |
| Total | 99.64 | 94.63 | 98.12 | 100.09 | 100.31 | 101.01 | 100.61 | 100.25 | 98.70 | 99.77 |
| ppm | | | | | | | | | | |
| Cr | nd | 4945 | 2641 | 5.0 | 118.0 | - | 156 | 311.0 | 38.0 | nd |
| Ni | 20.0 | 1025.7 | 961.2 | 13.0 | 37.0 | 194.0 | 82 | 115.0 | 40.0 | 2.0 |
| Sc | 9.8 | 24.9 | 16.9 | 26.0 | 22.3 | 55.0 | 47.6 | 47.4 | 54.7 | 26.0 |
| V | 75.0 | 73.9 | 132.4 | 78.0 | 170.6 | 271.0 | 281.5 | 242.9 | 262.0 | 107.0 |
| Pb | - | nd | 2.3 | - | 11.7 | - | 9.2 | 8.8 | 5.6 | - |
| Rb | 75.0 | 0.9 | 0.1 | 21.7 | 41.5 | 4.4 | 4 | 20.9 | 14.1 | 4.9 |
| Sr | 34.0 | 28.4 | 8.1 | 14.0 | 524.1 | 90.0 | 507.2 | 197.5 | 363.6 | 442.0 |
| Ba | 412.0 | 532 | 7 | 91.0 | 67.0 | 43.0 | 113 | 103.0 | 162.0 | 95.0 |
| Ga | 28.0 | 5.9 | 7.1 | 27.0 | 29.1 | 15.0 | 18 | 22.5 | 27.2 | 13.0 |
| Nb | 7.7 | 0.8 | 2.3 | 14.4 | 7.2 | 1.2 | 3.4 | 6.9 | 14.3 | 5.4 |
| Zr | 190.0 | 13.8 | 13.3 | 264.0 | 116.6 | 24.4 | 57.9 | 162.1 | 241.8 | 161.0 |
| Y | 12.9 | 13.9 | 10.9 | 14.0 | 30.5 | 12.6 | 23.3 | 33.2 | 52.1 | 20.1 |
| Th | - | nd | 1.2 | - | 11.1 | - | 1.1 | 6.4 | 4.5 | - |
| U | - | nd | nd | - | 2.4 | - | nd | 2.5 | 3.1 | - |
| ppm | | | | | | | | | | |
| La | - | 8 | 16 | 2.0 | 41.0 | 3.0 | 4.0 | 32.0 | 46.0 | 46.0 |
| Ce | 2.0 | nd | 11 | 20.0 | 78.0 | - | 10.0 | 69.0 | 87.0 | 92.0 |
| Nd | - | 7 | 1 | 5.0 | 33.0 | 4.0 | 4.0 | 33.0 | 46.0 | 36.0 |
| Cu | - | 17.8 | 24.9 | - | 9 | - | 123 | 67 | 529 | - |
| Zn | - | 95.6 | 185.7 | - | 44 | - | 105 | 129 | 96 | - |
| Co | - | 59.2 | 96.9 | - | 62.5 | - | 67 | 77.6 | 61.8 | - |

Analysis by X-ray fluorescence in the University of Adelaide on a Philips PW 1480 X-ray spectrometer. Major element analysis after Norrish and Hutton (1969). Trace element analysis: unignited powder mixed with binder and pressed into a pellet. Elements not analysed are marked '-' those with concentrations below detection limits are marked 'nd' and have detection limits of approximately 3.5, 2, 2, 5, 5.5 ppm for Pb, Th, U, Ce, Cr, respectively. $Fe_2O_3^*$ total iron represented as $Fe_2O_3$. Analyses from: 853- Sullivan, 1985; 857- Aouker, 1985; 950-, 962-, HR91- this study.

Table 2
Selected brief petrographic descriptions of supracrustal rocks of the Entia gneiss complex

| | Qtz | Pl | Cpx | Hbl | Oam | Ms | Bt | Grt | St | Ky | Ep | Chl | Rt | Opaques | Crd | Misc |
|---|---|---|---|---|---|---|---|---|---|---|---|---|---|---|---|---|
| 890-8 | X | Z | | X | X | 1° | X | | P | P | | Rbt | X | 1 | | |
| 853-93 | X | Z | | X | X | | X | | X | P | X | R | X | | | apatite |
| 890-16 | X | Z | | X | X | | | | P | X | | | X | X | | |
| HR91-2 | X | Z | | X | | 2° | X | | X | P | | Rhbl | X | | | allanite |
| 891-11 | | Z | | X | | | | | P | P | | Rhbl | X | X | | |
| 890-5A | X | Z | | X | | 2° | | | X | X | X | Rhbl | X | X | | zircon, apatite |
| 853-97 | X | Z | | X | | | X | | | P | | Rbt | X | | | |
| 85-72 | X | Z | | X | | 2° | | | P | | X | Rhbl | X | X | | zircon |
| 962-131m | X | Z | | X | | | | | X | | | | | X | | |
| 891-8 | | Z | | X | | 2° | | | P | | | | X | X | | corundum, zircon, apatite |
| 950-077 | X | Z | | X | X | | | P | X | | | | X | X | | |
| HR91-8 | X | Z | | X | | 2° | | P | X | | X | Rhbl | X | X | | |
| HR91-22 | X | Z | | X | X | | | X | | | | | | X | | apatite |
| NA-6 | X | Z | | X | | | | P | | | | Rhbl | | X | | |
| 853-180 | X | Z | X | X | | | | P | | | | | | X | | apatite |
| HR91-20 | X | Z | | X | | | | P | | | | | | X | | allanite, apatite |
| HR91-21 | X | Z | | X | | | | P | | | | R | | X | | apatite |
| 853-16 | X | Z | | X | | | | P | | | | | X | X | | zircon, apatite |
| HR91-10 | X | Z | | X | | | X | P | | | | Rbt | | X | | apatite |
| 962-17 | X | Z | | X | X | | | | | | | | X | 1 | | |
| 962-017r | | Z | | X | | | | | | | X | X | X | X | | |
| 853-180 | X | Z | X | X | | | | | | | X | | | X | | titanite |
| 853-27 | X | Z | | | | | X | P | | | | | | X | | zircon |
| 85-75 | X | Z | | | | 1° | X | P | | P | | | X | X | | zircon |
| 962-11 | X | Z | | | | | X | | | fibrolite | | | | | | |
| 962-017b | X | Z | | | | 2° | X | | | P | | | X | | | |
| 853-77 | | Z | | | | 1° | X | | P | P | | Rbt | X | X | | corundum |
| 853-102 | | Z | | X | | 2° | X | P | | | | R | | X | | |
| 85-77 | X | Z | | | | 1°, 2° | | X | P | | | | X | | | zircon, apatite |
| 950-47 | X | Z | | X | X | 2° | | | | | | R | X | | X | zircon, allanite |
| 950-047a | X | Z | | X | X | 2° | | | | P | | | X | | X | |
| 950-84 | X | Z | | | X | | | | | P | | R | X | | X | titanite, zircon |
| 853-74 | X | Z | | | X | | X | | | P | | Rbt | | | X | zircon |
| 853-30 | X | Z | | | X | | X | | | X | | Rbt | X | 1 | X | zircon |
| 950-00A | X | Z | | | | | | | | X | | | X | | X | apatite |
| 950-098 | X | Z | | | | 2° | X | | | P | | | X | X | X | zircon |
| 950-081 | | | | | X | | | | | | | X | X | X | | talc, apatite |
| 950-089 | | | | X | X | | | | | | | X | X | X | | talc, apatite |

Abbreviations: X phase present, Z zoned, 1° primary phase, 2° secondary phase, P porphyroblastic, R retrograde, Rbt retrograde after biotite, Rhbl retrograde after hornblende, 1 one oxide only (i.e. not the usual exsolved ilmenite/titaniferous magnetite–ulvöspinel).

Table 3
Selected analyses of phases from the Harts Range

| | NA-06 | | | | | HR91-5 | | | | | | | HR91-8 | | | | | | | | HR91-20 | | | HR91-21 | | |
|---|---|---|---|---|---|---|---|---|---|---|---|---|---|---|---|---|---|---|---|---|---|---|---|---|---|---|
| | Hbl | Hbl | Pl | Grt | Grt | Cpx.core | Cpx | Cpx | Hbl | Hbl | Grt | Grt | Hbl | Hbl | Hbl | Pl | St | Grt | Grt | Grt | Pl | Hbl | Grt | Grt | Pl | Hbl |
| | * | * | | * | * | | @ | @ | * | * | *@ | *@ | * | * | * | | | * | * | * | | * | * | * | | * |
| SiO2 | 43.33 | 43.15 | 56.89 | 38.77 | 38.73 | 48.87 | 50.24 | 50.67 | 39.74 | 40.18 | 38.14 | 38.06 | 41.16 | 40.66 | 40.47 | 46.02 | 27.58 | 39.45 | 39.51 | 39.16 | 48.34 | 39.75 | 38.87 | 38.96 | 62.19 | 43.00 |
| TiO2 | 0.76 | 0.82 | 0.00 | 0.09 | 0.00 | 0.05 | 0.00 | 0.06 | 0.12 | 0.05 | 0.00 | 0.01 | 0.65 | 0.16 | 0.42 | 0.07 | 0.78 | 0.02 | 0.00 | 0.01 | 0.05 | 0.20 | 0.08 | 0.00 | 0.00 | 0.18 |
| Al2O3 | 15.53 | 15.55 | 28.15 | 22.29 | 22.63 | 0.15 | 0.70 | 0.87 | 12.84 | 12.16 | 22.72 | 21.90 | 18.39 | 18.86 | 18.97 | 35.14 | 51.84 | 23.18 | 23.21 | 23.01 | 33.56 | 19.97 | 22.33 | 23.02 | 21.40 | 15.95 |
| FeO | 17.22 | 17.16 | 0.14 | 25.83 | 26.08 | 42.06 | 20.35 | 20.67 | 26.98 | 26.44 | 30.80 | 32.77 | 15.40 | 15.83 | 15.10 | 0.00 | 12.86 | 27.80 | 26.31 | 25.94 | 0.18 | 18.09 | 28.01 | 29.66 | 0.00 | 15.50 |
| MnO | 0.42 | 0.27 | 0.22 | 2.23 | 4.23 | 0.39 | 0.20 | 0.53 | 0.41 | 0.34 | 1.88 | 2.23 | 0.16 | 0.29 | 0.34 | 0.00 | 0.13 | 1.81 | 1.84 | 2.09 | 0.02 | 0.36 | 2.12 | 1.70 | 0.22 | 0.18 |
| MgO | 9.14 | 8.96 | 0.00 | 2.72 | 2.55 | 8.29 | 7.25 | 7.35 | 3.89 | 4.38 | 1.17 | 1.12 | 9.86 | 8.70 | 9.87 | 0.00 | 3.40 | 6.80 | 6.73 | 5.95 | 0.00 | 7.51 | 3.53 | 5.98 | 0.00 | 10.96 |
| CaO | 11.42 | 11.52 | 9.72 | 9.69 | 9.36 | 1.05 | 20.96 | 20.40 | 10.69 | 10.76 | 7.49 | 6.95 | 10.17 | 10.72 | 10.65 | 18.08 | 0.02 | 4.02 | 5.42 | 5.59 | 16.32 | 10.66 | 6.99 | 3.64 | 3.21 | 9.64 |
| Na2O | 1.40 | 1.36 | 6.16 | 0.00 | 0.27 | 0.00 | 0.00 | 0.08 | 1.50 | 1.33 | 0.00 | 0.00 | 0.92 | 1.04 | 1.43 | 0.83 | 0.04 | 0.00 | 0.00 | 0.00 | 2.25 | 1.50 | 0.00 | 0.00 | 2.17 | 1.28 |
| K2O | 0.72 | 0.70 | 0.00 | 0.00 | 0.00 | 0.03 | 0.02 | 0.08 | 1.97 | 1.82 | 0.00 | 0.04 | 0.24 | 0.14 | 0.31 | 0.00 | 0.03 | 0.00 | 0.05 | 0.00 | 0.00 | 0.29 | 0.00 | 0.00 | 9.46 | 0.19 |
| Cr2O3 | | | | | | | | | | | | | | | | | 0.03 | | | | | | | | | |
| ZnO | | | | | | | | | | | | | | | | | 0.71 | | | | | | | | | |
| Total | 99.95 | 99.49 | 101.27 | 101.61 | 103.83 | 100.88 | 99.71 | 100.70 | 98.13 | 97.45 | 102.20 | 103.08 | 96.95 | 96.40 | 97.56 | 100.14 | 97.4 | 103.09 | 103.07 | 101.75 | 100.72 | 98.33 | 101.93 | 102.96 | 98.65 | 96.88 |
| Si | 6.32 | 6.32 | 2.52 | 3.00 | 2.96 | 1.99 | 1.98 | 1.98 | 6.29 | 6.38 | 2.98 | 2.98 | 6.09 | 6.07 | 5.98 | 2.11 | 7.710 | 2.97 | 2.97 | 2.99 | 2.20 | 5.91 | 3.00 | 2.96 | 2.86 | 6.35 |
| Ti | 0.08 | 0.09 | 0.00 | 0.01 | 0.00 | 0.00 | 0.00 | 0.00 | 0.01 | 0.01 | 0.00 | 0.00 | 0.07 | 0.02 | 0.05 | 0.00 | 0.164 | 0.00 | 0.00 | 0.00 | 0.00 | 0.02 | 0.00 | 0.00 | 0.00 | 0.02 |
| Al | 2.67 | 2.68 | 1.47 | 2.03 | 2.04 | 0.01 | 0.03 | 0.04 | 2.40 | 2.28 | 2.09 | 2.02 | 3.21 | 3.32 | 3.30 | 1.90 | 17.082 | 2.06 | 2.06 | 2.07 | 1.80 | 3.50 | 2.03 | 2.07 | 1.16 | 2.78 |
| Fe2+ | 2.10 | 2.10 | 0.01 | 1.67 | 1.67 | 1.43 | 0.67 | 0.67 | 3.57 | 3.51 | 2.01 | 2.14 | 1.91 | 1.98 | 1.86 | 0.00 | 3.007 | 1.75 | 1.66 | 1.65 | 0.01 | 2.25 | 1.81 | 1.89 | 0.00 | 1.92 |
| Mn | 0.05 | 0.03 | 0.01 | 0.15 | 0.27 | 0.01 | 0.01 | 0.02 | 0.05 | 0.05 | 0.12 | 0.15 | 0.02 | 0.04 | 0.04 | 0.00 | 0.030 | 0.12 | 0.12 | 0.14 | 0.00 | 0.04 | 0.14 | 0.11 | 0.01 | 0.02 |
| Mg | 1.99 | 1.96 | 0.00 | 0.31 | 0.29 | 0.50 | 0.43 | 0.43 | 0.92 | 1.04 | 0.14 | 0.13 | 2.17 | 1.94 | 2.17 | 0.00 | 1.416 | 0.76 | 0.75 | 0.68 | 0.00 | 1.66 | 0.41 | 0.68 | 0.00 | 2.41 |
| Ca | 1.78 | 1.81 | 0.46 | 0.80 | 0.77 | 0.05 | 0.89 | 0.85 | 1.81 | 1.83 | 0.63 | 0.58 | 1.61 | 1.72 | 1.68 | 0.89 | 0.006 | 0.32 | 0.44 | 0.46 | 0.80 | 1.70 | 0.58 | 0.30 | 0.16 | 1.53 |
| Na | 0.40 | 0.39 | 0.53 | 0.00 | 0.04 | 0.00 | 0.00 | 0.01 | 0.46 | 0.41 | 0.00 | 0.00 | 0.27 | 0.30 | 0.41 | 0.07 | 0.020 | 0.00 | 0.00 | 0.00 | 0.20 | 0.43 | 0.00 | 0.00 | 0.19 | 0.37 |
| K | 0.13 | 0.13 | 0.00 | 0.00 | 0.00 | 0.00 | 0.00 | 0.00 | 0.40 | 0.37 | 0.00 | 0.00 | 0.04 | 0.03 | 0.06 | 0.00 | 0.009 | 0.00 | 0.00 | 0.00 | 0.00 | 0.05 | 0.00 | 0.00 | 0.56 | 0.04 |
| Cr | | | | | | | | | | | | | | | | | 0.006 | | | | | | | | | |
| Zn | | | | | | | | | | | | | | | | | 0.146 | | | | | | | | | |
| Total | 15.53 | 15.51 | 5.00 | 7.98 | 8.04 | 4.00 | 4.00 | 4.00 | 15.92 | 15.86 | 7.97 | 8.01 | 15.39 | 15.41 | 15.56 | 4.97 | 29.596 | 7.99 | 8.00 | 7.98 | 5.00 | 15.57 | 7.98 | 8.00 | 4.93 | 15.44 |
| XFe | 0.51 | 0.52 | - | 0.84 | 0.85 | 0.74 | 0.61 | 0.61 | 0.80 | 0.77 | 0.94 | 0.94 | 0.47 | 0.51 | 0.46 | - | 0.68 | 0.70 | 0.69 | 0.71 | - | 0.57 | 0.82 | 0.74 | - | 0.44 |

Analyses carried out at CEMMSA, using a JEOL 733 Electron Probe Microanalyser with the support of Mr Huw Rosser. Labelled analyses used in geothermometry using the mineral pair: *=hbl–gt, #=gt–bt, @=cpx–gt (for results for geothermometry see Table 4). Analyses used in average $P$ calculations using the method of Powell and Holland (1988): t1, t2.

Table 3 (continued)

| | HR91-22 | | | | | | | 853-16 | | | | 853-55 | | | | | | | | | | | HR91-10 | | |
|---|---|---|---|---|---|---|---|---|---|---|---|---|---|---|---|---|---|---|---|---|---|---|---|---|---|
| | Hbl | Hbl | Hbl | Pl | Grt | Grt | Oam | Hbl | Pl | Grt | St | Hbl | Hbl | Hbl | Hbl | Pl | Grt | Grt | Grt | Grt | Bt | Bt | Bt | Pl | Grt |
| | * | * | * | | * | * | | * | | * | | * | * | * | * | | * | * | * | *# | # | # | # | | # |
| SiO2 | 43.97 | 42.57 | 42.99 | 59.26 | 39.43 | 39.15 | 47.35 | 42.06 | 52.64 | 38.83 | 28.07 | 39.35 | 39.98 | 39.41 | 39.58 | 47.78 | 38.39 | 38.56 | 38.37 | 38.21 | 35.78 | 35.06 | 36.90 | 62.54 | 38.61 |
| TiO2 | 0.49 | 0.69 | 0.50 | 0.03 | 0.00 | 0.00 | 0.24 | 0.49 | 0.19 | 0.12 | 0.72 | 0.23 | 0.31 | 0.21 | 0.57 | 0.14 | 0.00 | 0.10 | 0.03 | 0.05 | 2.31 | 2.73 | 1.45 | 0.00 | 0.10 |
| Al2O3 | 14.66 | 15.23 | 15.43 | 25.62 | 22.70 | 23.00 | 11.47 | 16.70 | 30.73 | 22.82 | 53.46 | 17.74 | 17.05 | 16.73 | 16.89 | 31.84 | 22.22 | 22.15 | 22.33 | 22.14 | 18.56 | 18.84 | 18.52 | 23.49 | 22.72 |
| FeO | 15.00 | 14.13 | 14.85 | 0.04 | 28.34 | 28.48 | 19.40 | 17.17 | 0.09 | 29.92 | 13.05 | 19.23 | 18.61 | 20.72 | 20.08 | 0.21 | 23.82 | 27.09 | 27.59 | 27.55 | 19.99 | 18.80 | 14.19 | 0.00 | 28.43 |
| MnO | 0.37 | 0.34 | 0.45 | 0.05 | 1.67 | 1.98 | 0.35 | 0.32 | 0.17 | 1.11 | 0.10 | 0.77 | 0.42 | 0.52 | 0.57 | 0.00 | 7.11 | 4.36 | 4.30 | 3.55 | 0.13 | 0.18 | 0.34 | 0.17 | 5.55 |
| MgO | 12.28 | 11.24 | 10.89 | 0.00 | 7.31 | 7.17 | 16.71 | 9.41 | 0.00 | 6.00 | 2.86 | 6.74 | 7.47 | 6.50 | 6.90 | 0.86 | 2.41 | 3.28 | 3.71 | 3.86 | 9.79 | 9.96 | 13.95 | 0.00 | 5.31 |
| CaO | 9.47 | 10.05 | 9.81 | 6.92 | 2.92 | 2.86 | 0.78 | 11.08 | 12.69 | 4.82 | 0.04 | 11.32 | 11.04 | 11.09 | 11.32 | 15.45 | 7.31 | 6.32 | 6.19 | 6.54 | 0.22 | 0.33 | 0.32 | 4.60 | 1.42 |
| Na2O | 1.43 | 1.36 | 1.26 | 7.19 | 0.00 | 0.00 | 0.20 | 1.20 | 4.09 | 0.00 | 0.01 | 0.54 | 0.98 | 0.76 | 0.99 | 3.04 | 0.00 | 0.00 | 0.00 | 0.00 | 0.00 | 0.00 | 0.00 | 8.60 | 0.00 |
| K2O | 0.10 | 0.20 | 0.14 | 0.00 | 0.00 | 0.00 | 0.00 | 0.47 | 0.00 | 0.03 | 0.02<br>0.03<br>0.61 | 1.07 | 0.83 | 1.09 | 1.06 | 0.00 | 0.07 | 0.00 | 0.00 | 0.00 | 9.46 | 8.77 | 7.23 | 0.03 | 0.00 |
| Total | 97.76 | 95.81 | 96.33 | 99.10 | 102.39 | 102.63 | 96.51 | 98.89 | 100.59 | 103.65 | 99.0 | 95.92 | 95.85 | 95.93 | 96.91 | 99.32 | 101.33 | 101.85 | 102.52 | 101.91 | 96.23 | 94.67 | 92.90 | 99.42 | 102.14 |
| Si | 6.43 | 6.35 | 6.38 | 2.66 | 2.99 | 2.97 | 6.90 | 6.19 | 2.37 | 2.94 | 7.706 | 6.01 | 6.09 | 6.06 | 6.02 | 2.21 | 3.00 | 3.00 | 2.97 | 2.97 | 2.70 | 2.67 | 2.77 | 2.78 | 2.98 |
| Ti | 0.05 | 0.08 | 0.06 | 0.00 | 0.00 | 0.00 | 0.03 | 0.05 | 0.01 | 0.01 | 0.149 | 0.03 | 0.04 | 0.02 | 0.06 | 0.00 | 0.00 | 0.01 | 0.00 | 0.00 | 0.13 | 0.16 | 0.08 | 0.00 | 0.01 |
| Al | 2.53 | 2.68 | 2.70 | 1.35 | 2.03 | 2.06 | 1.97 | 2.90 | 1.63 | 2.04 | 17.301 | 3.20 | 3.06 | 3.03 | 3.03 | 1.74 | 2.05 | 2.03 | 2.04 | 2.03 | 1.65 | 1.69 | 1.64 | 1.23 | 2.07 |
| Fe2+ | 1.83 | 1.76 | 1.84 | 0.00 | 1.80 | 1.81 | 2.36 | 2.11 | 0.00 | 1.90 | 2.996 | 2.46 | 2.37 | 2.67 | 2.55 | 0.01 | 1.56 | 1.76 | 1.78 | 1.79 | 1.26 | 1.20 | 0.89 | 0.00 | 1.84 |
| Mn | 0.05 | 0.04 | 0.06 | 0.00 | 0.11 | 0.13 | 0.04 | 0.04 | 0.01 | 0.07 | 0.023 | 0.10 | 0.05 | 0.07 | 0.07 | 0.00 | 0.47 | 0.29 | 0.28 | 0.23 | 0.01 | 0.01 | 0.02 | 0.01 | 0.36 |
| Mg | 2.68 | 2.50 | 2.41 | 0.00 | 0.83 | 0.81 | 3.63 | 2.06 | 0.00 | 0.68 | 1.170 | 1.53 | 1.70 | 1.49 | 1.56 | 0.06 | 0.28 | 0.38 | 0.43 | 0.45 | 1.10 | 1.13 | 1.56 | 0.00 | 0.61 |
| Ca | 1.48 | 1.61 | 1.56 | 0.33 | 0.24 | 0.23 | 0.12 | 1.75 | 0.61 | 0.39 | 0.012 | 1.85 | 1.80 | 1.83 | 1.85 | 0.77 | 0.61 | 0.53 | 0.51 | 0.54 | 0.02 | 0.03 | 0.03 | 0.22 | 0.12 |
| Na | 0.41 | 0.39 | 0.36 | 0.63 | 0.00 | 0.00 | 0.06 | 0.34 | 0.36 | 0.00 | 0.006 | 0.16 | 0.29 | 0.23 | 0.29 | 0.27 | 0.00 | 0.00 | 0.00 | 0.00 | 0.00 | 0.00 | 0.00 | 0.74 | 0.00 |
| K | 0.02 | 0.04 | 0.03 | 0.00 | 0.00 | 0.00 | 0.00 | 0.09 | 0.00 | 0.00 | 0.008<br>0.006<br>0.123 | 0.21 | 0.16 | 0.21 | 0.21 | 0.00 | 0.01 | 0.00 | 0.00 | 0.00 | 0.91 | 0.85 | 0.69 | 0.00 | 0.00 |
| Total | 15.47 | 15.45 | 15.41 | 4.98 | 7.99 | 8.00 | 15.11 | 15.53 | 4.99 | 8.03 | 29.499 | 15.55 | 15.57 | 15.61 | 15.65 | 5.05 | 7.98 | 7.98 | 8.01 | 8.01 | 7.79 | 7.75 | 7.68 | 4.98 | 7.98 |
| XFe | 0.41 | 0.41 | 0.43 | - | 0.68 | 0.69 | 0.39 | 0.51 | - | 0.74 | 0.72 | 0.62 | 0.58 | 0.64 | 0.62 | - | 0.85 | 0.82 | 0.81 | 0.80 | 0.53 | 0.51 | 0.36 | - | 0.75 |

| | 853-27 | | | | 85-72 | | | 950-077 | | | | | 950-047 | | | | | 950-081 | | | | 853-30 | |
|---|---|---|---|---|---|---|---|---|---|---|---|---|---|---|---|---|---|---|---|---|---|---|---|
| | Grt | Grt | Bt | Bt | Hbl | St | Pl | St | Hbl | Oam | Grt | Pl | Tcl | Crd | Pl | Hbl | Chl | Chl | Hbl | Tlc | Oam | Oam | Crd |
| | # | # | # | # | | | | t2 | t1,2 | t1 | t1,2 | t1,2 | | | | | | | | | | | |
| SiO2 | 38.71 | 38.73 | 36.98 | 36.03 | 40.18 | 26.62 | 47.02 | 29.20 | 42.02 | 41.72 | 38.47 | 57.88 | 57.90 | 50.65 | 47.31 | 47.04 | 25.99 | 31.37 | 55.80 | 57.68 | 57.82 | 44.68 | 49.56 |
| TiO2 | 0.00 | 0.00 | 1.20 | 1.04 | 0.80 | 0.46 | 0.00 | 0.47 | 0.57 | 0.03 | 0.01 | 0.09 | 0.00 | 0.02 | 0.03 | 0.47 | 0.00 | 0.18 | 0.20 | 0.00 | 0.00 | 0.20 | 0.00 |
| Al2O3 | 22.43 | 22.31 | 17.04 | 17.07 | 19.70 | 53.10 | 34.75 | 54.46 | 16.00 | 17.94 | 22.58 | 25.86 | 3.86 | 33.74 | 39.00 | 14.97 | 21.72 | 16.20 | 0.68 | 0.24 | 0.52 | 19.23 | 34.02 |
| FeO | 24.94 | 25.80 | 11.43 | 10.48 | 13.91 | 11.75 | 0.13 | 12.47 | 14.68 | 19.62 | 29.31 | 0.28 | 3.65 | 2.15 | 0.02 | 6.72 | 7.15 | 3.63 | 2.35 | 3.95 | 8.08 | 13.41 | 2.61 |
| MnO | 4.38 | 2.64 | 0.11 | 0.10 | 0.48 | 0.28 | 0.12 | 0.12 | 0.16 | 0.34 | 1.74 | 0.06 | 0.21 | 0.00 | 0.00 | 0.23 | 0.21 | 0.00 | 0.15 | 0.07 | 0.75 | 0.43 | 0.16 |
| MgO | 9.63 | 9.45 | 18.89 | 17.40 | 10.37 | 3.16 | 0.00 | 3.00 | 10.69 | 14.20 | 6.10 | 0.00 | 28.55 | 11.65 | 0.00 | 16.16 | 28.58 | 30.84 | 22.63 | 26.54 | 28.90 | 18.75 | 11.36 |
| CaO | 2.23 | 2.62 | 0.41 | 1.12 | 10.59 | 0.02 | 16.99 | 0.02 | 9.81 | 0.70 | 3.16 | 7.48 | 0.22 | 0.17 | 0.30 | 11.21 | 0.00 | 0.20 | 12.38 | 0.32 | 0.50 | 0.74 | 0.29 |
| Na2O | 0.93 | 0.48 | 1.94 | 1.61 | 2.29 | 0.01 | 1.52 | 0.01 | 1.35 | 1.09 | 0.00 | 6.68 | 0.00 | 0.00 | 7.19 | 0.75 | 1.73 | 0.00 | 0.00 | 0.00 | 0.00 | 1.13 | 0.00 |
| K2O | 0.00 | 0.02 | 7.63 | 7.00 | 0.29 | 0.01<br>0.04<br>0.19 | 0.00 | 0.02<br>0.02<br>0.39 | 0.09 | 0.00 | 0.00 | 0.00 | 0.00 | 0.22 | 0.35 | 0.06 | 0.00 | 0.00 | 0.00 | 0.03 | 0.00 | 0.00 | 0.00 |
| Total | 103.25 | 102.05 | 95.63 | 91.84 | 98.60 | 95.6 | 100.53 | 100.2 | 95.37 | 95.64 | 101.38 | 98.33 | 94.4 | 98.6 | 94.2 | 97.6 | 85.37 | 82.42 | 94.19 | 88.83 | 96.57 | 98.6 | 98.0 |
| Si | 2.92 | 2.94 | 2.70 | 2.72 | 5.86 | 7.520 | 2.14 | 7.867 | 6.30 | 6.20 | 2.97 | 2.62 | 3.78 | 5.05 | 2.21 | 6.60 | 2.58 | 2.67 | 7.91 | 3.99 | 7.94 | 6.23 | 4.99 |
| Ti | 0.00 | 0.00 | 0.07 | 0.06 | 0.09 | 0.098 | 0.00 | 0.095 | 0.06 | 0.00 | 0.00 | 0.00 | 0.00 | 0.00 | 0.00 | 0.05 | 0.00 | 0.01 | 0.02 | 0.00 | 0.00 | 0.02 | 0.00 |
| Al | 1.99 | 2.00 | 1.46 | 1.52 | 3.39 | 17.686 | 1.87 | 17.295 | 2.83 | 3.14 | 2.06 | 1.38 | 0.30 | 3.97 | 2.15 | 2.48 | 2.55 | 1.63 | 0.11 | 0.02 | 0.08 | 3.16 | 4.04 |
| Fe2+ | 1.57 | 1.64 | 0.70 | 0.66 | 1.70 | 2.777 | 0.00 | 2.808 | 1.84 | 2.44 | 1.89 | 0.01 | 0.20 | 0.18 | 0.00 | 0.79 | 0.59 | 0.26 | 0.28 | 0.23 | 0.93 | 1.56 | 0.22 |
| Mn | 0.28 | 0.17 | 0.01 | 0.01 | 0.06 | 0.068 | 0.00 | 0.027 | 0.02 | 0.04 | 0.11 | 0.00 | 0.01 | 0.00 | 0.00 | 0.03 | 0.02 | 0.00 | 0.02 | 0.00 | 0.09 | 0.05 | 0.01 |
| Mg | 1.08 | 1.07 | 2.05 | 1.96 | 2.25 | 1.330 | 0.00 | 1.204 | 2.39 | 3.14 | 0.70 | 0.00 | 2.78 | 1.73 | 0.00 | 3.38 | 4.24 | 3.92 | 4.78 | 2.74 | 5.91 | 3.89 | 1.70 |
| Ca | 0.18 | 0.21 | 0.03 | 0.09 | 1.66 | 0.006 | 0.83 | 0.005 | 1.58 | 0.11 | 0.26 | 0.36 | 0.02 | 0.02 | 0.02 | 1.69 | 0.00 | 0.02 | 1.88 | 0.02 | 0.07 | 0.11 | 0.03 |
| Na | 0.14 | 0.07 | 0.27 | 0.24 | 0.65 | 0.004 | 0.13 | 0.003 | 0.39 | 0.31 | 0.00 | 0.59 | 0.00 | 0.00 | 0.65 | 0.20 | 0.33 | 0.00 | 0.00 | 0.00 | 0.00 | 0.31 | 0.00 |
| K | 0.00 | 0.00 | 0.71 | 0.67 | 0.05 | 0.003<br>0.008<br>0.040 | 0.00 | 0.005<br>0.004<br>0.078 | 0.02 | 0.00 | 0.00 | 0.00 | 0.00 | 0.03 | 0.02 | 0.01 | 0.00 | 0.00 | 0.00 | 0.00 | 0.00 | 0.00 | 0.00 |
| Total | 8.16 | 8.10 | 8.00 | 7.92 | 15.71 | 29.539 | 4.99 | 29.31 | 15.43 | 15.39 | 8.00 | 4.97 | 7.07 | 10.98 | 5.05 | 15.220 | 10.310 | 8.503 | 15.009 | 7.003 | 15.021 | 15.327 | 10.994 |
| XFe | 0.59 | 0.61 | 0.25 | 0.25 | 0.43 | 0.68 | - | 0.70 | 0.44 | 0.44 | 0.73 | - | 0.07 | 0.09 | - | 0.19 | 0.12 | 0.06 | 0.06 | 0.08 | 0.14 | 0.286 | 0.114 |

complex forms the basement complex (observed as the core of the dome) beneath a cover sequence (the Irindina supracrustal assemblage), which experienced a separate metamorphic and deformational history before being juxtaposed with the Entia gneiss complex in thrust duplexes co-incident with the intrusion of the syn-tectonic, mylonitised Bruna gneiss at 1747±3 Ma (Cooper et al., 1988). The structurally overlying Irindina supracrustal assemblage comprises the Harts Range meta-igneous complex with pelitic, semi-pelitic, carbonate and other minor lithologies which show evidence of repeated fold generations (Ding and James, 1985). The first of these fold generations resulted in the formation of a micaceous schistosity in amphibolite-grade pelites and tectonic layering and a mineral lineation in amphibolite, quartzite and calcareous lithologies. The common nature of the amphibolite metamorphism to both the Entia gneiss and the Irindina supracrustal assemblage suggests that these sequences were juxtaposed prior to or during amphibolite facies metamorphism.

The supracrustal assemblages found as lenses within the dominant intrusive felsic magmas of the Entia Dome have provided suitable compositions for the development of a large array of metamorphic assemblages and form the basis for this study. In particular, we will focus on a band of supracrustals occurring in the northeastern quadrant of the Entia Dome. These rocks contain only rare evidence of the pre-existing granulite facies equilibria and the phase relations dealt with in this contribution concern almost entirely the subsequent amphibolite facies metamorphism. The discontinuous layer (up to ~20 m thick) of supracrustal material outcropping in the northeastern Entia Dome exhibits a relatively consistent internal stratigraphy involving an association of calc-silicates (including a pink manganiferous epidote rock), porphyroblastic garnet amphibolites, garnet–kyanite–biotite schists, and gedrite gneisses. The layer extends over a distance of several kilometres, suggesting that some semi-continuous character is retained by the supracrustal sequence of the Entia gneiss complex. Although strongly boudinaged and disrupted by the intrusive felsic gneisses, such layers form mappable horizons which show evidence of multiple fold generations (Ding and James, 1985 and Fig. 1). The whole-rock chemistry, petrography and mineral chemistry of these supracrustal rocks are discussed below (Tables 1, 2 and 3, respectively).

## 3. Rock chemistry, petrography and mineral chemistry

### 3.1. Biotite-rich rocks

Bulk-rock analyses of porphyroblastic kyanite–biotite schists from the Entia Dome (Table 1) show that these rocks are $SiO_2$- and $K_2O$-poor, but $Al_2O_3$-rich in comparison to true pelitic rocks (cf. Hudson and Harte, 1985). The association of this rock type with migmatites adjacent to intrusive units (Buick, 1983) suggests that they may be restitic material associated with partial melting of pelitic or quartzo-feldspathic rocks in the kyanite stability field. Elongate kyanite grains contain straight inclusion trails and are sub-parallel to the biotite foliation which wraps around them. This implies that the kyanite is syn-deformational. In some samples kyanite is pseudomorphed by fibrous sillimanite. Minor proportions of quartz, plagioclase hornblende and muscovite occur in these rocks. Garnet porphyroblasts are also wrapped by the biotite foliation and in several examples garnet is in contact with kyanite (Fig. 2a). Biotite and garnet show substantial variation in chemistry. Biotite is most magnesian in association with kyanite and more Fe-rich with garnet or hornblende with a wide range of $X_{Fe}$ (=Fe/(Fe+Mg), 0.13–0.45) and has tschermakite substitution ($Mg, Fe_{-1}Si_{-1}Al_1Al_1$, from annite) in the range 0.25–0.33. Garnet ($X_{Fe}$ 0.63–0.77) is also more Fe-rich in hornblende-bearing schists. Plagioclase is calcium rich andesine ($X_{An}$=Ca/(Ca+Na), 0.31–0.32).

### 3.2. Magnesium-rich rocks

Two types of magnesium-rich rocks occur in the Entia Dome, both typified by low CaO and alkali contents (Table 1), but distinguishable by

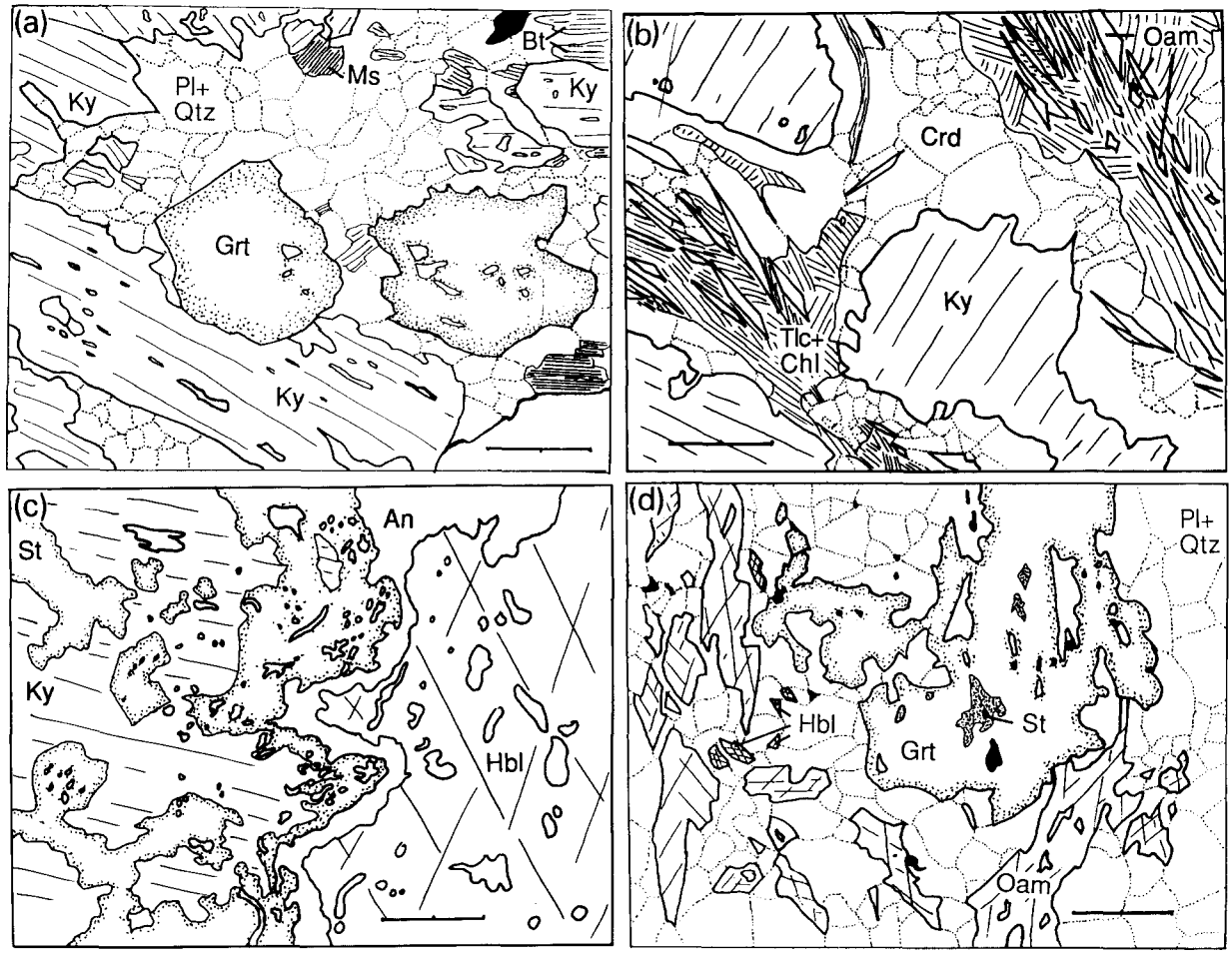


Fig. 2. Mineral textures in rocks from the Harts Range. (a) Euhedral garnet and kyanite poikiloblasts in a muscovite biotite schist (85/75). (b) Coarse, fresh cordierite separating corroded relic kyanite and acicular anthophyllite which is being replaced by chlorite and talc (853-74). (c) Aluminous enclave of coarse, corroded relic kyanite rimmed by staurolite and anorthite in a hornblende–plagioclase–quartz matrix (891-011). (d) Staurolite inclusion in garnet porphyroblast in a hornblende–gedrite–plagioclase matrix (950-077). Abbreviations: *Als*=aluminosilicate; *An*=anorthite; *Bt*=biotite; *Crd*=cordierite; *Chl*=chlorite; *Cpx*=clinopyroxene; *Ep*=epidote; *Grt*=garnet; *Hbl*=hornblende; *Ky*=kyanite; *Ms*=muscovite; *Oam*=orthoamphibole; *Pl*=plagioclase; *Qtz*=quartz; *Rt*=rutile; *St*=staurolite; *Tlc*=talc; *V*=vapour. Scale bar=2 mm.

their relative aluminium bulk-rock contents. Low-alumina magnesium-rich rocks occur as isolated pods and have bulk chemistries (including trace element chemistry; samples 950-081, 950-089, Table 1) broadly consistent with mafic or ultramafic intrusive, cumulate or xenolithic origins. Their low CaO and $Al_2O_3$ contents and high FeO, MgO, Cr and Ni (cf. Sivell et al., 1985) imply an orthopyroxene cumulate protolith. The hydrated mineral associations occurring in these rocks involve magnesio-anthophyllite–tremolite(or magnesio-hornblende)–talc–chlorite with minor biotite, plagioclase, magnetite, rutile and zircon (amphibole nomenclature after Leake, 1978). Anthophyllite ($X_{Fe}$ 0.12–0.27), tremolite ($X_{Fe}$ 0.06–0.1) and magnesio-hornblende ($X_{Fe}$ 0.24–0.25) form euhedral diamond-shaped grains or laths which are surrounded by acicular to fine talc ($X_{Fe}$ 0.07–0.1, $X_{ts}$ (Al on octahedral site) 0.01–0.04) and chlorite ($X_{Fe}$ 0.06–0.16, $X_{ts}$

0–0.22), which tend to form radiating sheaves. Rare intergrown biotite occurs in minor proportions.

The more aluminous Mg-rich rocks are dominated by cordierite and have a bulk chemistry which is comparable to that of the "whiteschists" described by Schreyer (1973) (Table 1, sample 853-39). As noted by previous authors (e.g. McKie, 1959; Robinson and Jaffe, 1969; Chinner and Fox, 1974) these rocks are compositionally unlike any common sedimentary or igneous rock type (having high Al-content but comparatively very low Ca, K and Fe). A chemically similar sedimentary rock type may result from the deposition of sediments in an evaporitic environment (Schreyer, 1977). Alternative sources for "whiteschist" type rocks include hydrothermal alteration (Vallance, 1967) or metasomatism (Tilley, 1937), erosion (with a chemical weathering component) of mafic igneous rocks (Robinson and Jaffe, 1969) or partial melting of a more typical rock type (Robinson and Jaffe, 1969). The sporadic occurrence of these bodies suggests that these rock types were not originally laterally extensive and, with the lack of associated shallow-water meta-sediments, is not consistent with deposition in an evaporitic environment. They are not consistently associated with igneous bodies, nor do they contain evidence of high-temperature metamorphism or partial melts and thus a restitic origin can be discounted. The cordierite-bearing rocks contain variable amounts of rounded zircon grains and coarse apatite (0.5–2%) and they typically contain abundant rutile. The high apatite and zircon contents and relatively little Cr and Ni (Table 1) of these rocks is consistent with a felsic rather than mafic origin. Sapphirine granulites from the Strangways Range to the west of this area have a similar chemistry (Windrim et al., 1984). The field relations and widely variable REE concentrations of these rocks were correlated with an abundance of minor phases such as zircon, sphene and apatite which were attributed to precipitation during hydrothermal alteration (Windrim et al., 1984). In the Entia Dome this association of cordierite-bearing Mg–Al-rich rocks is also consistent with an origin involving hydrothermally altered felsic rocks, which may have experienced chloritisation (addition of magnesium, removal of silica, calcium and alkalis) and, by correlation with the Strangways examples, possible mobilisation of trace elements before metamorphism.

The classification of the bulk chemistry of these rocks as "whiteschists" does not extend to their mineralogy which by definition must involve the assemblage kyanite–talc (Schreyer, 1973). Whereas kyanite is present as elongate, skeletal porphyroblasts (Fig. 2b) sub-parallel to the orthoamphibole, biotite or hornblende foliation, it is never observed with similarly oriented talc. Kyanite and amphibole (hornblende and anthophyllite) are never observed in contact and kyanite is corroded with optically continuous relic grains surrounded by coarse, relatively fresh cordierite. These rims of cordierite separating kyanite from anthophyllite and hornblende suggest that the rocks experienced the reactions:

kyanite + anthophyllite ⇒ cordierite

kyanite + hornblende ⇒ cordierite

(in the presence of plagioclase, quartz, vapour). While kyanite, hornblende and orthoamphibole define a weak foliation, cordierite is coarse-grained, randomly oriented and undeformed and is therefore thought to have developed subsequent to the foliation-forming deformation. Fine intergrowths of talc and chlorite are randomly oriented among corroded amphiboles and cross-cut the coarse cordierite grains. Quartz, plagioclase, rutile and apatite are subordinate and zircons are relatively coarse and abundant (up to 0.3 mm). All of the ferro-magnesian minerals occurring in these cordierite rocks are very Mg-rich ($X_{FeHbl}$ 0.16–0.27, $X_{FeOam}$ 0.07–0.1, $X_{FeCrd}$ 0.07–0.08, $X_{FeTlc}$ 0.07–0.17, Table 3) and the amphiboles show limited edenite substitution in contrast to associated rock types. The proportion of tschermakite molecule in both clino- and ortho-amphiboles is high in comparison to those in other assemblages.

### 3.3. Amphibolites

Amphibolites in the Entia Dome have variable bulk compositions and mineralogy. The

typical hornblende–plagioclase–epidote (±clinopyroxene±cummingtonite) amphibolites correspond to basaltic compositions which contain significant $Na_2O$ ($\geq 1.3$ wt%), while others show depletion or enrichment in other elements (Table 1). These clinopyroxene-bearing amphibolites are typically found in relatively undeformed zones (e.g. boudins) and are the only samples to show relict granulite facies phases. Some of the less common amphibolites have unusually high CaO and MgO in comparison to their high $SiO_2$ and $Al_2O_3$ contents (e.g. sample 853-16), suggesting that they have experienced a complex chemical evolution. The relatively high contents of rare earth elements (REE) of these unusual high-Ca–Mg amphibolites in comparison to the "basaltic" types suggest that they do not have a cumulate origin. This is because the incompatible REE would be expected to partition into the melt fraction of any solid–liquid system, depleting the cumulates in REE in comparison to the undifferentiated "basalts". It is likely that the rocks have rather experienced some chemical alteration, and because the observed reaction textures may be simply interpreted in terms of closed system divariant equilibria in CFMASH we consider that they do not result from extensive metasomatism, but probably from alteration at the sea floor. The bulk chemistry of these unusual amphibolites exerts some control on their mineralogy. Lower $Na_2O$ and CaO allow unusual assemblages involving hornblende–staurolite–kyanite–orthoamphibole±quartz or corundum, and for Fe-rich samples, hornblende–garnet to develop, rather than the "common" assemblage often observed in basaltic rocks (cf. Gibson, 1978; Laird, 1980; Selverstone et al., 1984).

The less calcic and sodic staurolite- and kyanite-bearing amphibolites often preserve evidence of incomplete reactions in the form of coronas and overgrowths and thus are potentially useful in determining the metamorphic history of the rocks. Kyanite typically forms embayed porphyroblasts which are surrounded by a moat of staurolite inside a rim of anorthitic plagioclase to form aluminous coronas separating the weakly aligned kyanite from the hornblende–plagioclase±orthoamphibole mosaic which makes up the bulk of the rock (Fig. 2c). These textures suggest the reaction:

kyanite + hornblende ⇒ staurolite
+ anorthite (+quartz + vapour)

Commonly all kyanite is consumed leaving large grains of staurolite which are rimmed by anorthite–bytownite plagioclase in a hornblende–plagioclase±orthoamphibole mosaic. In rocks which do not contain quartz, corundum occurs rarely in small optically continuous aggregates rimmed with anorthite and in contact with staurolite in an amphibolite matrix suggesting a reaction of the form:

corundum + hornblende ⇒ staurolite
+ anorthite

Coarse, euhedral orthoamphibole is observed in contact with hornblende, often cross-cutting both the hornblende-defined foliation and also the hornblende grains themselves. Gedrite is never observed as inclusions in any other phase (except cordierite in Mg-rich rocks).

In a number of Fe-rich amphibolites, garnet also occurs as euhedral porphyroblasts typically 0.25–20 mm in diameter, up to 20 m in diameter! The porphyroblasts often contain large inclusions of plagioclase, quartz, hornblende and titanium phases which show straight to slightly curved inclusion trails. Rutile occurs in the cores of garnet porphyroblasts, but decreases in abundance and is replaced by ilmenite toward the rims. Staurolite and garnet co-exist in several samples. Staurolite occurs as amoeboid inclusions at the core of a very coarse garnet (Fig. 2d), which shows weak inclusion trails parallel to the external hornblende–orthoamphibole–plagioclase (in equilibrium with garnet) foliation, we interpret this texture as evidence of the divariant reaction:

hornblende + staurolite ⇒ garnet
(+quartz, plagioclase, vapour)

Chlorite and biotite are observed to replace hornblende, chlorite grows over biotite and

hornblende is sometimes replaced by the low-temperature assemblage titanite–epidote–prehnite.

Microprobe analyses (WDS) of staurolites show that Zn does not appear to play a role in the stabilisation of staurolite (staurolites contain 0.12–0.77 wt% ZnO ≡ 0.02–0.15 ZnO per formula unit with 44O+4(OH)) and the mineral chemistry of the staurolites corresponds fairly closely with the "normal" ranges reported by Ribbe (1985). This implies that its presence in such a rare assemblage must be related to the phase relations of mafic rocks and varying physical conditions rather than its unusual chemistry. Staurolite in these amphibolites are unzoned and have well defined compositions, these being more Fe-rich with garnet ($X_{Fe}$ 0.69–0.83) and more magnesian in rocks which contain only hornblende and/or gedrite as ferro-magnesian phases ($X_{Fe}$ 0.52–0.71).

Garnet in these amphibolites is generally almandine-rich ($X_{alm}$ 0.51–0.7, $X_{prp}$ 0.1–0.36, $X_{sps}$ 0.04–0.16, $X_{grs}$ O.04–0.22), unzoned and consistent within each sample. The analyses show no evidence of substitution of $Fe^{3+}$, Ti or Cr for Si or Al. Coexisting garnet and staurolite show reversed Fe–Mg partitioning, i.e. $X_{Fe,St}$ (0.69–0.83) > $X_{Fe,Grt}$ (0.66–0.74), in comparison to typical rocks of pelitic affinity (e.g. Sharma and MacRae, 1981; Spear, 1982; Arnold and Sandiford, 1990). This may be due to the changing chemical relationship of iron and magnesium in garnet and staurolite with increasing pressure (A. Purvis, pers. commun., 1991) or possibly the continued reaction of one phase in isolation from the other (Grew and Sandiford, 1985).

Hornblende is pargasitic to tschermakitic (Leake, 1978) and contains up to 0.9 atoms of $Na_2O$ per 23 oxygens. It generally has an $X_{Fe}$ less than that of co-existing garnet, staurolite and orthoamphibole and greater than coexisting biotite and chlorite, in the range 0.21–0.77. The orthoamphibole in amphibolites is gedrite, which exhibits substantial edenite and tschermakite substitution (0–0.53 Na per formula unit, $X_{ts}$ 0.62–1.56). Gedrite shows no evidence of exsolution lamellae (even at the micron scale) and there is only one orthoamphibole present at all times.

The composition of plagioclase in amphibolites from the Entia Dome shows systematic variation with the nature of the assemblage in which it occurs. Typically matrix plagioclase is weakly zoned, with cores several percent richer in albite than the rims (i.e. reverse zoning). The most calcic plagioclase (bytownite–anorthite) co-exists with staurolite, while the plagioclase occurring with hornblende, orthoamphibole or epidote tends to be andesine. The most sodic plagioclases (oligoclase) occur with garnet. Epidote is generally a solid solution between clinozoisite and epidote, with 30–90% epidote end-member in amphibolites bearing other aluminous phases such as staurolite, kyanite or gedrite. Kyanite from the Entia Dome amphibolites contains < 0.64% $Fe_2O_3$ and < 0.1% MnO.

The order of Fe-enrichment in amphibolites is staurolite > garnet > gedrite > hornblende > biotite > chlorite.

## 4. Conditions of metamorphism

### 4.1. Geothermometry

The wide variety of rocks occurring in the supracrustal assemblage of the Entia gneiss complex provides an opportunity to constrain its thermal history using a number of different geothermometers. A selection of calibrations of Fe and Mg cation exchange in garnet–hornblende (Graham and Powell, 1984; Powell, 1985), garnet–biotite (Thompson, 1976; Ferry and Spear, 1978; Hodges and Spear, 1982) and garnet–clinopyroxene (Powell, 1985) pairs have been used to constrain the peak metamorphic conditions of equilibria in rocks from the Entia Dome. Calculated temperatures were in the range 570–710°C at an assumed pressure of 5 kbar (see Table 4) and somewhat higher in samples which showed signs of retrogression (sample 853-55 640–778°C). These are considered to be minimum estimates for peak temperatures, and show substantial variation (14–99°C) between different pairs of analyses in the same sample. This

Table 4
Temperature estimates made using Fe–Mg partitioning for garnet–hornblende, garnet–biotite and garnet–clinopyroxene

| Grt-Hbl | NA-6 | NA-6 | 853-16 | HR91-5 | HR91-5 | HR91-8 | HR91-8 |
|---|---|---|---|---|---|---|---|
| XFeHbl | 0.51 | 0.52 | 0.51 | 0.80 | 0.77 | 0.47 | 0.46 |
| XFeGrt | 0.84 | 0.85 | 0.74 | 0.94 | 0.94 | 0.70 | 0.71 |
| XCaGrt | 0.29 | 0.28 | 0.13 | 0.23 | 0.20 | 0.11 | 0.16 |
| ln Kd | 1.618 | 1.678 | 1.005 | 1.332 | 1.575 | 0.963 | 1.049 |
| T(°C) G&P2 | 647 | 628 | 665 | 664 | 585 | 660 | 685 |
| T(°C) G&P | 673 | 654 | 692 | 690 | 614 | 688 | 710 |

| Grt-Hbl | HR91-20 | HR91-21 | HR91-22 | HR91-22 | HR91-22 | HR91-22 |
|---|---|---|---|---|---|---|
| XFeHbl | 0.57 | 0.44 | 0.41 | 0.41 | 0.43 | 0.43 |
| XFeGrt | 0.82 | 0.74 | 0.69 | 0.69 | 0.69 | 0.69 |
| XCaGrt | 0.21 | 0.10 | 0.08 | 0.08 | 0.08 | 0.08 |
| ln Kd | 1.192 | 1.253 | 1.179 | 1.150 | 1.046 | 1.071 |
| T(°C) G&P2 | 685 | 571 | 569 | 576 | 602 | 595 |
| T(°C) G&P | 711 | 602 | 607 | 607 | 632 | 626 |

| Grt-Bt | HR91-10 | 853-27 | 853-27 |
|---|---|---|---|
| Xann | 0.36 | 0.25 | 0.25 |
| Xalm | 0.63 | 0.51 | 0.53 |
| Xpy | 0.21 | 0.35 | 0.35 |
| Xgrs | 0.04 | 0.06 | 0.07 |
| Xsps | 0.12 | 0.09 | 0.05 |
| ln K(ideal) | -1.661 | -1.454 | -1.512 |
| T(°C) F&S | 602 | 683 | 659 |
| T(°C) T | 597 | 639 | 625 |
| T(°C) H&S | 618 | 706 | 687 |

| Grt-Cpx | HR91-5 | HR91-5 |
|---|---|---|
| XFeCpx | 0.61 | 0.61 |
| XFeGrt | 0.94 | 0.94 |
| XCaGrt | 0.23 | 0.20 |
| ln Kd | 2.236 | 2.338 |
| T(°C) P | 621 | 581 |

Temperature estimates for assumed pressure 5 kbar are near independent of pressure (varying by ~5°C/kbar). Abbreviations: garnet–hornblende (G&P2) the updated method of Graham and Powell (1984) (Powell, 1985); (G&P) Graham and Powell (1984); garnet–biotite: (F&S) Ferry and Spear (1978); (T) Thompson (1976); (H&S) Hodges and Spear (1982); Clinopyroxene–garnet (Powell, 1985).

may be a function of the samples equilibrating at different times due to partial re-equilibration or variations in grainsize.

### 4.2. Average-pressure calculations

The results of average-pressure calculations by the method of Powell and Holland (1988) are

presented in Table 5 for adjacent staurolite–garnet–hornblende and hornblende–garnet–gedrite assemblages in sample 950-077. Compositions of staurolite and hornblende inclusions in garnet and the garnet core compositions were used to establish average pressures for the core assemblage at 5.4 kbar for an assumed temperature of 600°C. The matrix assemblage hornblende–garnet–gedrite equilibrated at a calculated pressure of 6.7 kbar for an assumed temperature of 650°C. These conditions are consistent with the occurrence of kyanite.

Table 5
Average pressure calculations [a]

(a) 950-077 (inside gt) (for x(H2O) = 1.0)

| | q | H2O | ilm | ru | an | ab | tr | ftr |
|---|---|---|---|---|---|---|---|---|
| a | 1 | 1 | 1 | 1 | 0.377 | 0.62 | 0.0003 | 3.6E-05 |
| sd(a)/a | 0 | | 0 | 0 | 0.11644 | 0.05 | 1.1547 | 1.13707 |

| | hb | parg | ed | gl | cumm |
|---|---|---|---|---|---|
| a | 0.0264 | 0.0148 | 0.00095 | 9.5E-06 | 5.2E-06 |
| sd(a)/a | 0.42086 | 0.50889 | 0.84708 | 6.47524 | 8.77903 |

| | gr | py | alm | fst | mst |
|---|---|---|---|---|---|
| a | 0.00064 | 0.0125 | 0.244 | 0.232 | 0.009 |
| sd(a)/a | 0.75127 | 0.53073 | 0.15 | 0.2 | 0.57463 |

| T°C | 500 | 525 | 550 | 575 | 600 | 625 | 650 |
|---|---|---|---|---|---|---|---|
| av P | 4.5 | 4.7 | 4.9 | 5.2 | 5.4 | 5.6 | 5.9 |
| sd | 1.14 | 1.1 | 1.09 | 1.12 | 1.17 | 1.15 | 1.23 |
| f | 2.1 | 2 | 1.9 | 1.9 | 1.9 | 1.9 | 2 |

(b) 950-077 (outside gt) (for x(H2O) = 1.0)

| | q | H2O | ilm | ru | an | ab | ftr |
|---|---|---|---|---|---|---|---|
| a | 1 | 1 | 1 | 1 | 0.377 | 0.62 | 3.6E-05 |
| sd(a)/a | 0 | | 0 | 0 | 0.11644 | 0.05 | 1.13707 |

| | hb | parg | ed | gl | cumm | anth |
|---|---|---|---|---|---|---|
| a | 0.0264 | 0.0148 | 0.00095 | 9.5E-06 | 5.2E-06 | 0.00012 |
| sd(a)/a | 0.42086 | 0.50889 | 0.84708 | 6.47524 | 8.77903 | 1.7999 |

| | ged | gr | py | alm |
|---|---|---|---|---|
| a | 0.0171 | 0.00064 | 0.0125 | 0.244 |
| sd(a)/a | 0.46515 | 0.75127 | 0.53073 | 0.15 |

| T°C | 500 | 525 | 550 | 575 | 600 | 625 | 650 |
|---|---|---|---|---|---|---|---|
| av P | 4.8 | 5.1 | 5.4 | 5.9 | 6.2 | 6.4 | 6.7 |
| sd | 0.84 | 0.83 | 0.84 | 0.81 | 0.82 | 0.85 | 1.03 |
| f | 1.6 | 1.6 | 1.5 | 1.4 | 1.4 | 1.4 | 1.6 |

[a]Made using THERMOCALC 2.0β, Powell and Holland (1988) and the enlarged and updated dataset of Holland and Powell (1990). Activities calculated using mixing on sites. For amphiboles activity calculations ignore substitution on the tetrahedral sites (as suggested by R. Powell, pers. commun., 1992). For 95% confidence, fit (=sd(fit)) should be less than 1.39.

## 5. Theoretical phase relations

Investigation of the theoretical phase relations in model systems provides another avenue for interpreting complex textural relations in metamorphic rocks. Here we use theoretical phase relationships and $P$–$T$ projections or phase diagrams constructed from the thermodynamic dataset of Holland and Powell (1990) to constrain the nature of changes in $P$–$T$ conditions to cause the reactions inferred on the basis of the textural interpretation discussed above. We begin by considering the simple systems KFMASH ($K_2O$–FeO–MgO–$Al_2O_3$–$SiO_2$–$H_2O$) and (F)MASH (FeO–MgO–$Al_2O_3$–$SiO_2$–$H_2O$) appropriate to pelites and rocks of "whiteschist" character before considering the calcium-bearing systems appropriate to the amphibolites.

### 5.1. KFMASH

The KFMASH phase diagrams of Powell and Holland (1990) and Dirks et al. (1991) may be used to place a limit upon the prevailing conditions during the foliation development by comparing the equilibrium assemblages with those represented in the phase diagram. The presence of garnet in kyanite–biotite schists with muscovite, quartz and vapour implies that temperatures must have been greater than 660°C at pressures greater than the sillimanite–kyanite univariant reaction i.e. >6.5 kbar at the time of kyanite–garnet stability. The later replacement of kyanite by randomly oriented sillimanite suggests higher temperatures and/or lower pressures at some time after deformation.

### 5.2. (F)MASH

The broadly similar chemistry of the cordierite bearing rocks in the Entia gneiss complex to "whiteschists" (Schreyer, 1973, 1974) suggests that theoretical phase diagrams for the MASH system may be appropriate to the phase relations of these real rocks. Experimental work with emphasis on the stability of cordierite with changing physical conditions (Schreyer and Seifert, 1969) has been used to construct phase dia-

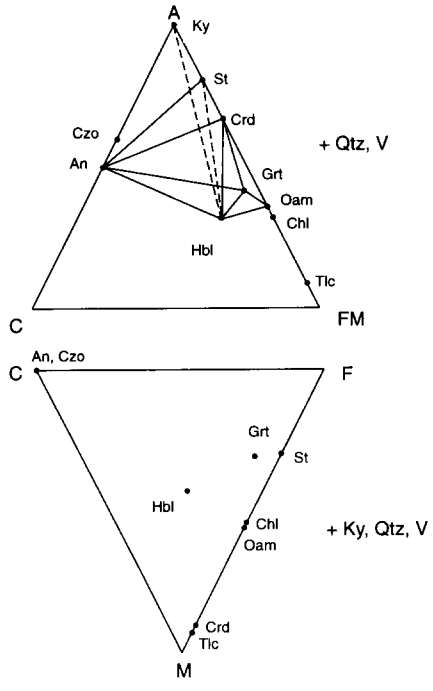


Fig. 3. The compositional relationships of phases in the compositional system CaO–FeO–MgO–$AlO_{3/2}$ shown as two sides of the tetrahedron. Upper triangle is constructed with quartz and aqueous vapour in excess, with FeO and MgO combined to show continuous reactions in CFMA as discontinuous in C(FM)A. Lower triangle shows the positions of phases on the CFM plane, i.e. projected from kyanite in addition to quartz and vapour. Dashed lines are unstable assemblages, solid lines represent stable assemblages. For abbreviations see Fig. 2.

grams for the MASH system appropriate to "whiteschists" (Schreyer, 1973, 1974) and chemically similar rock types. The original work of Schreyer and Seifert (1969), suggesting that the breakdown of anthophyllite and kyanite to produce cordierite takes place as a result of decreasing pressure from greater than about 10 kbar at temperatures $>800°C$, has been superseded by newer data suggesting that the appropriate pressure for this reaction is approximately 6 kbar at lower temperatures (Massone and Schreyer, 1983).

### 5.3. CFMASH

Because bulk-rock composition, along with pressure and temperature, is a strong factor in determining the reaction space of individual rocks, the variable bulk-rock chemistry of the amphibolites of the Entia gneiss complex provide an excellent opportunity to investigate the $P$–$T$ evolution. This is because most of the reactions experienced by a given rock are continuous and only rarely do individual rocks "see" discontinuous reactions. Since the $P$–$T$ conditions of continuous reactions are sensitive to bulk-rock compositional variation (particularly $X_{Fe}$) (Hensen, 1971), a group of rocks with grossly similar chemistry, but variable $X_{Fe}$ have the potential to preserve reaction textures at different stages of the $P$–$T$ history. The combination of $P$–$T$ segments deduced from individual rocks along with information about relative (and if possible absolute) timing with $P$–$T$ information may then be used to reconstruct the $P$–$T$ history of the region.

To illustrate the interdependence of the three parameters, $P$, $T$, $X$, it is useful to make sections through the $P$–$T$–$X$ diagram for a constant value of any one of the parameters (e.g. $T$–$X$ sections for constant pressure, $P$–$X$ sections for constant temperature or $P$–$T$ sections at constant composition). Phase diagrams which represent the effect of changing physical conditions for a specific bulk composition ($X$) are termed pseudosections (Powell, 1991). In the following section we outline the essential elements of petrological analysis of the Entia Dome amphibolites.

In order to develop a petrogenetic grid appropriate to the amphibolites we make the following approximations. While a large number of components are required to describe the chemistry of amphibolites ($NaO$–$CaO$–$FeO$–$MgO$–$Al_2O_3$–$SiO_2$–$H_2O$–$TiO_2$–$Fe_2O_3$–$MnO$–$K_2O$), the system is considerably simplified by taking account of phases in excess and neglecting those which are considered to be of minor importance. Thus, $TiO_2$ is present in significant amounts only in rutile and/or ilmenite (or titanite), while $Fe_2O_3$ is only found in magnetite and other $Fe^{3+}$-bearing spinels. $K_2O$ is present only in biotite. Since each of these components stabilizes only one phase they may be assumed to have no bearing on the reaction relationships between the other phases

and therefore can be ignored, reducing the components to NCFMASHMn. Similarly MnO occurs in only minor proportions in garnets and so is not considered essential. Sodium is clearly an important component in hornblende, orthoamphibole and plagioclase in the amphibolites. However, because many of the reaction textures involve anorthite-rich plagioclase we neglect the effect of $Na_2O$. We note that the phase relations in this simplified (CFMASH, Fig. 3) system may be schematically extended to the more complex NCFMASH system. This will have the effect of adding one degree of freedom to each of the reactions (thus, invariants become univariant and univariants become divariant), displacing the fields to stabilize those phases which partition $Na_2O$. The addition of $Na_2O$ to the CFMASH grid is expected to displace the various stability fields to higher pressure and lower temperature to stabilise plagioclase and orthoamphibole with respect to the other phases.

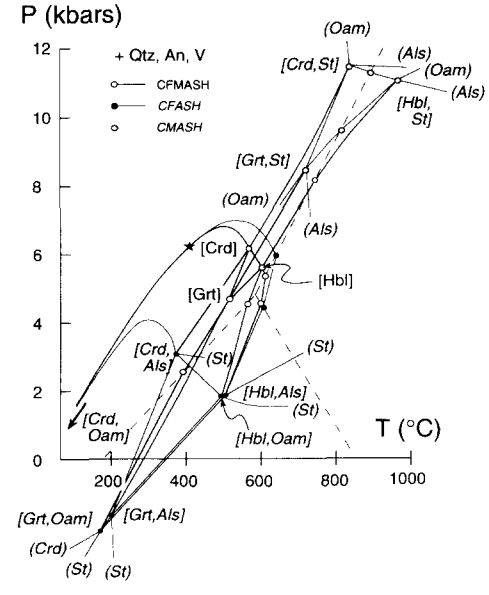


Fig. 4. A pressure–temperature projection for the system CFMASH, constructed with anorthite, quartz and an aqueous phase in excess (from J. Arnold, in prep.). Reactions are given in Table 6; star represents a singularity where, because of changing compositions, one or more phases switches sides. Note that the low-temperature portion of the diagram may be metastable with respect to chlorite. For abbreviations see Fig. 2.

Table 6
Reactions portrayed in Fig. 4

| | |
|---|---|
| CFASH: | |
| (Grt, Oam, Crd) | St + An + Qtz -> Hbl + Als + V |
| (Grt, Oam, St) | Hbl + Als + Qtz + V -> Crd + An |
| (Grt, Oam, Hbl) | St + Qtz -> Crd + Als + V |
| (Grt, Oam, Als) | St + Hbl + Qtz -> Crd + An |
| (Grt, Als, St) | Crd + Hbl + Qtz -> Oam + An + V |
| (Grt, Als, Hbl) | St + Oam + Qtz -> Crd + V |
| (Grt, Als, Crd) | St + Hbl + Qtz -> Oam + An + V |
| (Hbl, Als, St) | Grt + Qtz + V -> Crd + Oam + An |
| (Hbl, Als, Cd) | Grt + Qtz + V -> Oam + St + An |
| (Hbl, Als, Oam) | St + Grt + Qtz + V -> Crd + An |
| (Hbl, Oam, St) | Grt + Als + Qtz + V -> Crd + An |
| (Hbl, Oam, Crd) | Als + Grt + V -> St + An + Qtz |
| (Crd, Als, Oam) | Grt + Qtz + V -> Hbl + St + An |
| CMASH: | |
| (Grt, St, Oam) | Hbl + Als + Qtz + V -> Crd + An |
| (Grt, St, Als) | Hbl + Crd -> Oam + An + Qtz + V |
| (Grt, St, Crd) | Hbl + Als -> Oam + An + Qtz + V |
| (Grt, St, Hbl) | Als + Oam + Qtz + V-> Crd |
| (Hbl, St, Als) | Grt + Qtz + V -> Crd + Oam + An |
| (Hbl, St, Oam) | Grt + Als + Qtz + V -> Crd + An |
| (Hbl, St, Crd) | Grt + Qtz + V -> Als + Oam + An |
| (Crd, St, Oam) | Hbl + Als -> Grt + An + Qtz + V |
| (Crd, St, Als) | Grt + Qtz + V -> Oam + Hbl + An |
| CFMASH: | |
| (Grt, Oam) | Als + Hbl + Qtz + V -> Crd + St + An |
| (Grt, Als) | Hbl + St + Qtz -> Crd + Oam + An + V |
| (Grt, Hbl) | Als + Oam + Qtz + V-> St + Crd |
| (Grt, Crd) | St + Hbl + Qtz -> Als + Oam + An + V |
| (Crd, Oam) | Als + Grt + Hbl -> St + V + An + Qtz? |
| | Als + Grt + V -> Hbl + St + An + Qtz |
| (Crd, St) | Grt + Als + Hbl -> Oam + An + Qtz + V |
| (Crd, Hbl) | Als + Grt + V -> St + Oam + An + Qtz |
| (Hbl, St) | Oa + Als + An + Qtz + V -> Crd + Grt |
| (Hbl, Oam) | St + Crd + An + Qtz -> Grt + Als + V |
| (Hbl, Als) | St + Oam + An + Qtz -> Grt + Crd + V |
| (Grt, St) | Hbl + Als + Qtz + V -> Oam + Crd + An |

Reactions listed with higher pressure (or lower temperature for steep reactions) phases to the left of the equation. Reactions are labelled using the convention of bracketing the absent phases, e.g. (Crd, Grt). Reaction coefficients change along the length of the univariant reaction lines and so are not specified. Where two reactions are listed, the reaction involves a singularity and the lower temperature portion of the reaction is listed first.

In constructing the petrogenetic grid (Fig. 4) for the CFMASH system (involving the phases Ca-amphibole, anorthite feldspar, aluminosilicates, cordierite, garnet, orthoamphibole, staurolite, quartz and an aqueous vapour) we have used the computer program THERMOCALC version 2.0$\beta$ (Powell and Holland, 1988) and the internally consistent data set of Holland and Powell (1990). Quartz, aqueous vapour and an-

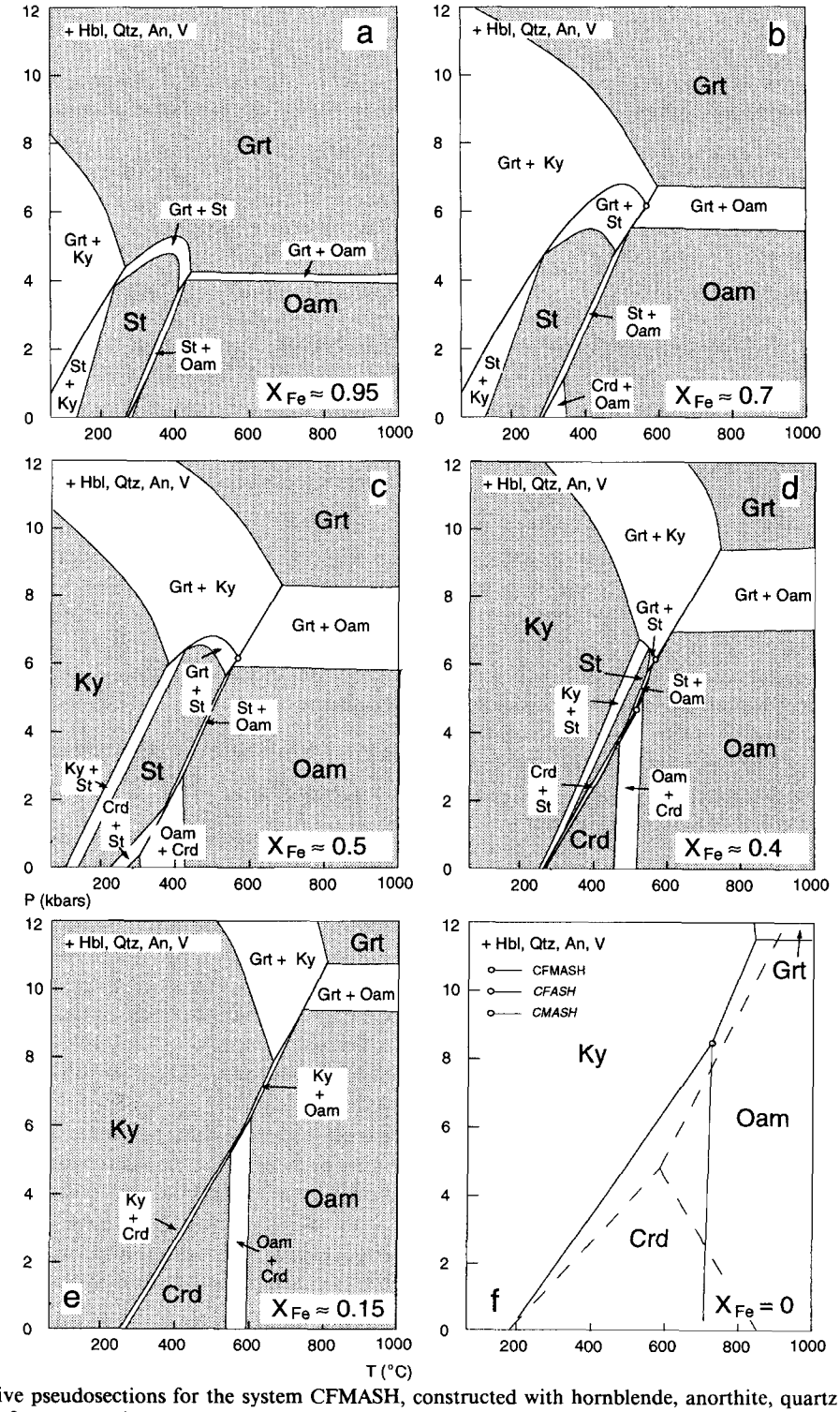


Fig. 5. Qualitative pseudosections for the system CFMASH, constructed with hornblende, anorthite, quartz and an aqueous vapour in excess for a range of bulk compositions (from J. Arnold, in prep.). For abbreviations see Fig. 2.

orthite are assumed to be in excess, thus precluding assemblages unsaturated in silica such as those which contain corundum; a detailed discussion of this and related phase diagrams is in preparation (J. Arnold, in prep.).

This phase diagram has been used to construct qualitative pseudosections for a range of bulk compositions, so that the reaction history of a range of real rocks can be evaluated. Pseudosections have been constructed for bulk compositions containing ubiquitous hornblende for a range of $X_{Fe}$ (Fig. 5; J. Arnold, in prep.). An excellent discussion on the construction and significance of pseudosections is provided by Powell and Holland (1990).

Fig. 5 shows predicted phase relations in the CFMASH system with excess hornblende, quartz, anorthite and aqueous vapour which change systematically with composition from a garnet–hornblende dominated mineralogy for very Fe-rich rocks to increasingly important orthoamphibole–hornblende assemblages at high temperatures and kyanite–hornblende at lower temperatures for more magnesian bulk compositions. Staurolite–hornblende and cordierite–hornblende assemblages are expected to be stable at low–intermediate temperatures for Fe-rich and Mg-rich bulk compositions, respectively.

## 6. The interpretation of changing physical conditions from metamorphic reaction textures

The combination of geothermometry, average-pressure calculations and theoretical phase relations for rocks in the Entia Dome may be used to constrain the *P–T* evolution of the amphibolite facies rocks. The majority of this information comes from theoretical phase relations which allow interpretation of the conditions of equilibration of successive assemblages rather than a single "peak" *P–T* point. In the discussion below, all assemblages are assumed to include excess hornblende, quartz, anorthite and vapour as they do in Fig. 5.

The presence of the foliation-forming assemblage hornblende–garnet in the most Fe-rich amphibolites from the Entia Dome reflects the large stability field of that assemblage for Fe-rich compositions. In rocks of this composition weakly aligned (pre- to syn-kinematic) inclusions of staurolite (and plagioclase, hornblende, quartz, ilmenite, rutile) in garnet porphyroblasts provide evidence that garnet–staurolite was stable at an earlier stage in the *P–T* evolution. This texture implies that syn-kinematic garnet grew in equilibrium with hornblende at the expense of staurolite and suggests that early *P–T* conditions placed the rock in the staurolite–hornblende trivariant or staurolite–garnet–hornblende divariant field, with later higher pressure and temperature conditions stabilising garnet–hornblende via the continuous reaction:

hornblende + staurolite ⇒ garnet

In other rocks of moderately high $X_{Fe}$, the presence of hornblende and plagioclase but no orthoamphibole inclusions in garnet, while hornblende–plagioclase–orthoamphibole occurs as an equilibrium assemblage in the foliated matrix, provides evidence of the continuous reaction:

garnet + hornblende ⇒ orthoamphibole + plagioclase

indicating re-equilibration at a lower pressure, as deformation continued. Orthoamphibole is often observed to cross-cut hornblende grains (and occasionally the foliation) indicating that although in equilibrium with hornblende, it developed slightly later in the syn- to post-kinematic stage. Due to the shallow slope of the divariant garnet–orthoamphibole (+hornblende, plagioclase, quartz, vapour) field, which limits orthoamphibole stability (Fig. 5b), the reaction must involve decreasing pressure from the garnet–hornblende to the garnet–orthoamphibole–hornblende or orthoamphibole–hornblende field.

Staurolite–anorthite coronas on kyanite grains, separating weakly foliated kyanite and hornblende, are probably due to the reaction:

kyanite + hornblende ⇒ staurolite + anorthite

This reaction reflects either an increase in pres-

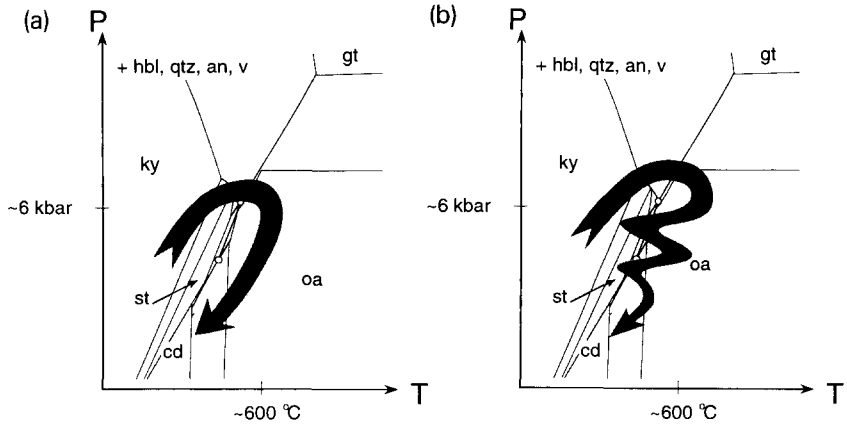


Fig. 6. Schematic *P–T* paths constructed using natural assemblages and the pseudosections of Fig. 5 resulting from (a) a single metamorphic event, and (b) multiple heating and cooling episodes. For abbreviations see Fig. 2.

sure and/or temperature in rocks of intermediate Fe content and due to the high surface energy of the texture, must have developed subsequent to the deformation.

Very Mg-rich rocks (containing hornblende, anorthite, quartz, vapour) bear evidence of a reaction involving the consumption of weakly aligned (syn-kinematic) hornblende and kyanite by cordierite. The appropriate pseudosections (Figs. 5e, 5f) suggest that this reaction may be most simply explained in terms of a decrease in pressure and/or an increase in temperature. The undeformed, random nature of the cordierite grains suggests that this reaction occurred in the post-kinematic stage. Another reaction observed in slightly more Fe-rich rock is the (post-kinematic) consumption of orthoamphibole and kyanite to produce cordierite (Fig. 5e). These reactions are most likely to result from decreasing temperature and pressure.

The sequences of reactions affecting rocks of different composition and occurring at different times in relation to the foliation development allow a relative chronology of *P–T* vectors to be established. This chronology may be used to distinguish between the different possibilities for the metamorphic history of the region.

If the amphibolite-grade reaction textures described above result from a single metamorphic event, this must have comprised a "clockwise" path involving: (1) an increase in pressure and temperature (kyanite⇒staurolite, staurolite⇒ garnet) from 5.4 kbar, 600°C (staurolite–garnet–plagioclase equilibria) through 6.7 kbar and 650°C (garnet–hornblende–orthoamphibole equilibria), to temperatures (570–710°C, estimated using conventional garnet–biotite, garnet–hornblende and clinopyroxene–garnet geothermometry, >6.5 kbar from co-existing garnet–kyanite–biotite in pelites) and perhaps higher pressures; (2) a decrease in pressure and, probably, temperature (garnet–hornblende⇒ orthoamphibole, kyanite + hornblende⇒ cordierite) (Fig. 6a). Decreasing pressure is also implied by the replacement of kyanite by sillimanite in pelites and the reactions (kyanite⇒ cordierite) and (orthoamphibole⇒ cordierite) reactions in potassium and calcium-poor (F)MASH rocks.

Alternatively, the reaction textures may result from multiple heating and cooling episodes at different pressures (Fig. 6b). In this scenario the reaction which stabilised garnet with respect to weakly foliated staurolite (now inclusions) corresponds to an early (syn-deformational) metamorphic event. Kyanite–hornblende and orthoamphibole–kyanite may also have developed during this period, the stabilisation of syn- to post-kinematic orthoamphibole with respect to hornblende and garnet reflecting a decrease in pressure subsequent to this. The corona texture involving kyanite–staurolite–anorthite (imply-

ing reaction under static conditions) would result from a further increase in temperature, with or without a change in pressure. Finally the late, coarse-grained cordierite (developed during strain-free periods and showing no evidence of later deformation) may be due to regional denudation.

The presence of low strain, up-temperature reaction textures involving kyanite–staurolite–anorthite coronas is not easily reconcilable with a single metamorphic cycle. This is because the statically developed (and therefore post-kinematic) kyanite–staurolite–anorthite coronas require lower temperatures of formation than the syn- to post-kinematic foliated orthoamphibole assemblages. (The possibility that the kyanite–staurolite–anorthite textures are miraculously preserved pre- rather than post-kinematic assemblages is discounted by the persistence of the high surface energy corona textures, which could be expected to undergo textural re-equilibration, with even a small amount of deformation.) Therefore the authors consider that this multiple phase metamorphic history provides a more satisfactory explanation of the textural relationships in rocks from the Harts Range than a single-cycle model.

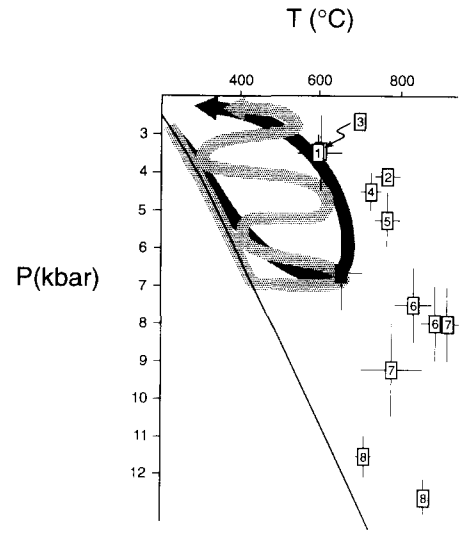


Fig. 7. A comparison of peak metamorphic conditions recorded in various central and northern Australian Proterozoic terranes and two possible $P$–$T$ paths for the Entia Dome plotted with reference to the stable continental geotherm of England and Thompson (1984) calculated for a thermal conductivity of 2 W $m^{-1}$ $K^{-1}$. Results from this paper shown in black; other areas: *1*=Tanami Block granites, Scrimgeour and Sandiford, 1993; *2*=Reynolds Range, Arunta Inlier, Dirks et al., 1991; *3*=Mary Kathleen Fold Belt, Mt Isa Inlier, Oliver et al., 1991; *4*=Anmatjira Range, Arunta Inlier, Hand et al., 1992; *5*=Broken Hill Block, Phillips, 1980; *6*=Strangways Range, Arunta Inlier, Warren, 1983; *7*=Strangways Range, Arunta Inlier, Goscombe, 1992b; *8*=Musgrave Range, Maboko et al., 1991.

## 7. Discussion

The assemblages described here show that while the Harts Range region and the eastern Arunta Inlier (Goscombe, 1992a, b) experienced granulite-grade metamorphism early in its history, in common with the remainder of the Arunta Inlier and other northern Australian Proterozoic terranes, its later evolution involved crustal reworking under much cooler thermal regimes (Fig. 7). The notable feature of this retrogressive kyanite-facies cycle(s) is its regional extent which contrasts the metamorphic reworking in other areas where either higher geothermal gradients were acting or where kyanite-bearing assemblages are restricted to very rare retrograde shear zones (e.g. Warren, 1983; Clarke et al., 1990).

Clearly the full significance of the amphibolite facies metamorphism in the Harts Range awaits a detailed evaluation of the mineral isotopic systems, a preliminary study of which is presented by Foden et al. (1995). We finish here with a brief discussion of the petrological data as it bears on the isotopic results of Foden et al. (1995).

Foden and co-workers (1992, 1995) have identified four distinct isotopic closure "events" in the eastern Arunta Inlier. The first of these relates to an episode of significant crustal growth involving the intrusion of both felsic and mafic magmas at granulite facies conditions at 1765–1735 Ma, which is recorded in U–Pb zircon systematics (Mortimer et al., 1987; Cooper et al., 1988) and in some Sm–Nd whole-rock isochrons, at 1780–1740 Ma. Foden et al. (1995) show that some Sm–Nd and Rb–Sr whole-rock isochrons and Sm–Nd mineral isochrons yield

ages in the vicinity of 1400–1500 Ma (e.g. 1463 ± 170 Ma). Similar ages have been determined from the Strangways region and Goscombe (1992a) has proposed that high-grade crustal reworking at this time caused re-equilibration of the isotopic systems. $^{40}Ar/^{39}Ar$ age spectra from muscovite porphyroclasts in the Ruby Gap duplex may also be correlated with this Mesoproterozoic resetting of the isotopic systems (> 1100 Ma, Dunlap et al., 1991). Sm–Nd systematics of garnet–hornblende pairs from the assemblages described here indicate that this assemblage either cooled through its closure temperature (~500–650°C, Foden et al., 1995) or formed at about 450 Ma. Rb–Sr isochrons in micas (closing at lower temperatures, approximately 500°C, Foden et al., 1995) preserve ages of 400–300 Ma. Similar ages have been reported from $^{40}Ar/^{39}Ar$ spectra for neocrystallised phengites (311–413 Ma) from Ruby Gap (Dunlap et al., 1991).

Since the time intervals between the various isotopic closure "events" obtained from the Entia gneiss complex (i.e. 240, 900 and 50 or more million years) are long in comparison to the thermal time constant of the lithosphere (the time required for the geotherm of thickened continental crust to return to the stable continental geotherm, which is thought to be of the order of 100 million years), it is unlikely that any of these events are causally related by a single cooling event affecting the whole region. Thus, it is probable that at least these isotopic events reflect distinct thermal episodes. Since the isotopic systems with the highest closure temperatures retain ages of about 1400 Ma and are correlated with the regional penetrative fabric, this age probably corresponds to the peak pressure and temperature conditions represented by garnet–hornblende equilibria. A further thermal perturbation at 450 Ma, sufficient to reset Sm–Nd mineral systematics, may be recorded in the mineral assemblages in the staurolite–anorthite coronas developed between earlier hornblende and kyanite. It is also likely that the substantial uplift elsewhere ascribed to the Alice Springs Orogeny (Collins and Teyssier, 1989) at ~300 Ma (and preserved in Rb–Sr mica cooling ages) is recorded in the Entia Dome amphibolites and may correspond to the coarse-grained cordierite developed between kyanite and hornblende and/or orthoamphibole and sillimanite replacing kyanite in pelites.

## 8. Conclusion

The petrographic evidence supporting repeated metamorphic heating episodes suggests that each of the isotopic "events" recorded in the Harts Range region may correlate with the development of one or more of the observed mineral textures. If this is the case it suggests that the eastern Arunta Inlier experienced a granulite facies history during the Palaeoproterozoic in common with other northern Australian inliers, but that it was subjected to substantial thermal perturbation and possibly crustal reworking in the Mesoproterozoic and possibly into the Palaeozoic.

## Acknowledgements.

Many thanks to Ian Scrimgeour and John Foden for comments made on an earlier draft and for helpful discussions. This paper has benefited from reviews by Bill Collins and Geoff Clarke. A careful, detailed and constructive review was also made by Ben Goscombe. We acknowledge Geoff Fraser for his assistance in the field and the Northern Territory Geological Survey for field support.

## References

Aouker, N., 1985. A Geological Review of the Southwest Entia Dome, With Emphasis on the Inkamulla Granite Gneiss, Harts Range, Eastern Arunta Block, Northern Territory. Honours Thesis, University of Adelaide, 28 pp. (unpubl.).

Arnold, J. and Sandiford, M., 1990. Petrogenesis of cordierite–orthoamphibole assemblages from the Springton Region, South Australia. Contrib. Mineral. Petrol., 106: 100–109.

Buick, I.S., 1983. The Geology, Petrology and Geochemistry

of the Huckitta Granodioritic Gneiss and Associated Granitoids, Harts Range, Central Australia. Honours Thesis, University of Adelaide, 28 pp. (unpubl.).

Buick, I.S., 1985.The Petrology of Granitic Rocks from the Entia Domal Structure, Eastern Arunta Block. M.Sc. Thesis, University of Adelaide, 149 pp. (unpubl.).

Chinner, G.A. and Fox, J.S., 1974. The origin of cordierite–anthophyllite rocks in the Land's End aureole. Geol. Mag., 111: 397–408.

Clarke, G.L., Collins, W.J. and Vernon, R.H., 1990. Successive overprinting granulite facies metamorphic events in the Anmatjira Range, central Australia. J. Metamorph. Geol., 8: 65–88.

Collins, W.J. and Teyssier, C., 1989. Crustal scale ductile fault systems in the Arunta Inlier, Central Australia. Tectonophysics, 158: 49–66.

Cooper, J.A., Mortimer, G.E. and James, P.R., 1988. Rate of Arunta Inlier evolution at the eastern margin of the Entia Dome, central Australia. Precambrian Res., 40/41: 233–259.

Ding, P. and James, P.R., 1985. Structural evolution of the Harts Range area and its implication for the development of the Arunta Block, central Australia. Precambrian Res., 27: 251–276.

Dirks, P.H.G.M., Hand, M. and Powell, R., 1991. The *P–T*-deformation path for a mid-Proterozoic, low-pressure terrane: the Reynolds Range, central Australia. J. Metamorph. Geol., 9: 641–661.

Dobos, S.K., 1978. Phase Relations, Element Distribution and Geochemistry of Metamorphic Rocks from the Eastern Arunta Block, NT. Ph.D. Thesis, Macquarie University, 313 pp. (unpubl.).

Dunlap, W.J., Teyssier, C., McDougall, I. and Baldwin, S., 1991. Ages of deformation from K/Ar and $^{40}Ar/^{39}Ar$ dating of white micas. Geology, 19: 1213–1216.

England, P.C. and Thompson, A.B., 1984. Pressure–temperature–time paths of regional metamorphism, I. Heat transfer during the evolution of regions of thickened continental crust. J. Petrol., 25: 894–928.

Etheridge, M.A., Rutland, R.W.R. and Wyborn, L.A.I., 1987. Orogenesis and tectonic processes in the early to middle Proterozoic of northern Australia. In: A. Kröner (Editor), Proterozoic Lithospheric Evolution. Am. Geophys. Union, Geodyn. Ser., 17: 131–147.

Ferry, J.M. and Spear, F.S., 1978. Experimental calibration of the partitioning of Fe and Mg between garnet and biotite. Contrib. Mineral. Petrol., 66: 113–117.

Foden, J.D., Buick, I.A. and Mortimer, G.E., 1988. The petrology and geochemistry of granitic gneisses from the East Arunta Inlier, central Australia: implications for Proterozoic crustal development. Precambrian Res., 40/41: 233–259.

Foden, J., Mawby, J., Arnold, J. and Sandiford, M., 1992. Constraints imposed by Nd–Sr isotopic and metamorphic studies on the crustal evolution of the E. Arunta Inlier. In: W.J. Collins (Editor), The Application of Geochronology to Field Related Geological Problems, SGGMP Workshop, Abstr. Geological Society of Australia. Alice Springs, N.T.

Foden, J., Mawby, J., Kelley, S., Turner, S. and Bruce, D., 1995. Metamorphic events in the eastern Arunta Inlier, Part 2. Nd–Sr–Ar isotopic constraints. In: W.J. Collins and R.D. Shaw (Editors), Time Limits on Tectonic Events and Crustal Evolution Using Geochronology: Some Australian Examples. Precambrian Res., 71: 207–227 (this volume).

Gibson, G., 1978. Staurolite in amphibolite and hornblendite sheets from the Upper Seaforth River, central Fiordland, New Zealand. Mineral. Mag., 42: 153–154.

Goscombe, B.D., 1992a. High-grade reworking of central Australian Granulites, Part 1. Structural evolution. Tectonophysics, 204: 361–399.

Goscombe, B.D., 1992b. High-grade reworking of central Australian Granulites: metamorphic evolution of the Arunta Complex. J. Petrol., 33: 917–962.

Graham, C.M. and Powell, R., 1984. A garnet–hornblende geothermometer: calibration, testing and application to the Pelona Schist, Southern California. J. Metamorph. Geol., 2: 13–31.

Grew, E.S. and Sandiford, M., 1985. Staurolite in a garnet–hornblende–biotite schist from the Lanterman range, northern Victoria Land, Antarctica. Neues Jahrb. Mineral., Monatsh., 9: 396–410.

Hand, M., Dirks, P.H.G.M., Powell, R. and Buick, I.S., 1992. How well established is isobaric cooling in Proterozoic orogenic belts? An example from the Arunta Inlier, central Australia. Geology, 20: 649–652.

Hensen, B.J., 1971. Theoretical phase relations involving cordierite and garnet in the system $MgO–FeO–Al_2O_3–SiO_2$. Contrib. Mineral. Petrol., 33: 191–214.

Hobbs, B.E., Archibold, N.J., Etheridge, M.A. and Wall, V.A., 1984. Tectonic history of the Broken Hill Block, Australia. In: A. Kröner and R. Greiling (Editors), Precambrian Tectonics Illustrated. E. Schweizerbart'sche Verlagsbuchhandlung, Stuttgart, pp. 353–369.

Hodges, K.V. and Spear, F.S., 1982. Geothermometry, geobarometry and the $Al_2SiO_5$ triple point at Mt Moosilauke, New Hampshire. Am. Mineral., 67: 1118–1134.

Holland, T.J.B. and Powell, R., 1990. An enlarged and updated internally consistent data set with uncertainties and correlations: the system $K_2O–Na_2O–CaO–MgO–MnO–FeO–Fe_2O_3–Al_2O_3–TiO_2–SiO_2–C–H_2–O_2$. J. Metamorph. Geol., 8: 89–124.

Hudson, N.F.C. and Harte, B., 1985. $K_2O$-poor, aluminous assemblages from the Buchan Dalradian, and the variety of orthoamphibole assemblages in aluminous bulk compositions in the amphibolite facies. Am. J. Sci., 285: 224–266.

James, P.R. and Ding, P., 1988. "Caterpillar tectonics" in the Harts Range area: a kinship between two sequential Proterozoic extension–collision orogenic belts within the eastern Arunta Inlier of central Australia. Precambrian Res., 40/41: 199–216.

Laird, J., 1980. Phase equilibria in mafic schist from Vermont. J. Petrol., 21: 1–37.

Leake, B., 1978. Nomenclature of amphiboles. Am. Mineral., 63: 1023–1052.

Loosveld, R.J.H. and Etheridge, M.A., 1990. A model for low-pressure facies metamorphism during crustal thickening. J. Metamorph. Geol., 8: 257–267.

Maboko, M.A.H, Williams, I.S. and Compston, W., 1991. Zircon U–Pb chronometry of the pressure and temperature history of granulites in the Musgrave Ranges, central Australia. J. Geol., 99: 675–697.

Massone, H.J. and Schreyer, W., 1983. Stability of the talc–kyanite assemblage revisited. Terra Cognita, 13: 187.

McKie, D., 1959. Yoderite, a new hydrous magnesium silicate from Mautia Hill, Tanganyiki. Mineral. Mag., 32: 282–307.

Mortimer, G.E., Cooper, J.A. and James, P.R., 1987. U–Pb and Rb–Sr geochronology and geological evolution of the Harts Range ruby mine area of the Arunta Inlier, central Australia. Lithos, 20: 445–467.

Norrish, K. and Hutton, J.T., 1969 An accurate x-ray spectrographic method for the analysis of a wide range of geological samples. Geochim. Cosmochim. Acta, 33: 431–453.

Oliver, N.H.S., Holcombe, R.J., Hill, E.J. and Pearson, P., 1991. Tectono-metamorphic evolution of the Mary Kathleen Fold Belt, northwest Queensland: a reflection of mantle plume processes? Aust. J. Earth Sci., 38: 425–455.

Phillips, G.N., 1980. Water activity changes across an amphibolite–granulite facies transition, Broken Hill, Australia. Contrib. Mineral. Petrol., 75: 377–386.

Powell, R., 1985. Regression diagnostics and robust regression in geothermometer/geobarometer calibration: the garnet–clinopyroxene geothermometer revisited. J. Metamorph. Geol., 3: 231–243.

Powell, R., 1991. Metamorphic Mineral Equilibria Short Course: Course notes. University of Melbourne.

Powell, R. and Holland, T.J.B., 1988. An internally consistent dataset with uncertainties and correlations, 3. Applications to geobarometry, worked examples and a computer program. J. Metamorph. Geol., 6: 173–204.

Powell, R. and Holland, T.J.B., 1990. Calculated mineral equilibria in the pelite system, KFMASH $K_2O$–FeO–MgO–$Al_2O_3$–$SiO_2$–$H_2O$. Am. Mineral., 75: 367–380.

Ribbe, P.H., 1985. Staurolite. In: P.H. Ribbe (Editor), Orthosilicates. Reviews in Mineralogy 5. The Mineralogical Society of America, Washington, D.C. pp. 171–188.

Robinson, P. and Jaffe, H.W., 1969. Aluminous enclaves in gedrite–cordierite gneiss from southwestern New Hampshire. Am. J. Sci., 267: 389–421.

Sandiford, M. and Powell, R., 1991. Some remarks on high-temperature–low-pressure metamorphism in convergent orogens. J. Metamorph. Geol., 9: 330–340.

Schreyer, W., 1973. Whiteschist: a high-pressure rock and its geological significance. J. Geol., 81: 735–739.

Schreyer, W., 1974. Whiteschist, a new type of metamorphic rock formed at high pressures. Geol. Rundsch., 63: 597–609.

Schreyer, W., 1977. Whiteschists, their compositions and pressure–temperature regimes based on experimental, field and petrographic evidence. Tectonophysics, 43: 127–144.

Schreyer, W. and Seifert, F., 1969. Compatibility relations of the aluminium silicates in the system MgO–$Al_2O_3$–$SiO_2$–$H_2O$ and $K_2O$–MgO–$Al_2O_3$–$SiO_2$–$H_2O$ at high pressures. Am. J. Sci., 267: 371–388.

Scrimgeour, I. and Sandiford, M., 1993. Early Proterozoic metamorphism at the Granites Gold Mine, Northern Territory: Implications for the timing of fluid production in the high-$T$, low-$P$ terrains. Econ. Geol., 88: 1099–1133.

Selverstone, J., Spear, F., Franz, G. and Morteani, G., 1984. High pressure metamorphism in the SW Tauern Window, Austria: $P$–$T$ paths from hornblende–kyanite–staurolite schists. J. Petrol., 25: 501–531.

Sharma, R.S. and MacRae, N.D., 1981. Paragenetic relations in gedrite–cordierite–staurolite–biotite–sillimanite–kyanite gneisses at Ajitpura, Rajasthan, India. Contrib. Mineral. Petrol., 78: 48–60.

Shaw, R.D., Stewart, A.J. and Black, L.P., 1984. The Arunta Inlier: a complex ensialic mobile belt in central Australia, Part 2. Tectonic history. Aust. J. Earth Sci., 31: 457–484.

Shaw, R.D., Freeman, M.J. and others, 1990. Quartz (1:100,000 scale geological map). Bureau of Mineral Resources, Canberra.

Sivell, W.J., Foden, J.D. and Lawrence, R.W., 1985. The Entire anorthositic gneiss, eastern Arunta Inlier, central Australia: geochemistry and petrogenesis. Aust. J. Earth Sci., 32: 449–465.

Spear, F.S., 1982. Phase equilibria of amphibolites from the Post Pond Volcanics, Mt Cube Quadrangle, Vermont. J. Petrol., 23: 383–426.

Stewart, A.J., Shaw, R.D. and Black, L.P., 1984. The Arunta Inlier: a complex ensialic mobile belt in central Australia, Part 1. Stratigraphy, correlations and origin. Aust. J. Earth Sci., 31: 445–455.

Sullivan, S.J., 1985 A Detailed Geological Investigation of the Entia Gneiss and Leucocratic Gneiss Intrusive, Northern Entia Dome, Harts Ranges, Eastern Arunta Block. Honours Thesis, University of Adelaide, 35 pp. (unpubl.).

Thompson, A.B., 1976. Mineral reactions in pelitic rocks, II. Calculation of some $P$–$T$–$X$(Fe–Mg) phase relations. Am. J. Sci., 267: 425–45.

Tilley, C.E., 1937. Anthophyllite–cordierite granulites of the Lizard. Geol. Mag., 74: 300–309

Vallance, T.G., 1967. Mafic rock alteration and isochemical development of some cordierite–anthophyllite rocks. J. Petrol., 8: 84–96.

Warren, R.G., 1983. Metamorphic and tectonic evolution of granulites, Arunta Block, central Australia. Nature, 305: 300–303.

Windrim, D.P., McCulloch, M.T., Chappel, B.W. and Cameron, W.E., 1984. Nd isotopic systematics and chemistry of Central Australian sapphirine granulites: an example of rare earth element mobility. Earth Planet. Sci. Lett., 70: 27–39.